JAMES | Journal of Advances in Modeling Earth Systems

RESEARCH ARTICLE
10.1029/2023MS004157

Key Points:

- Effect of continuum uncertainty on climate sensitivity is modest for a surface temperature of 288 K but substantial at higher temperatures
- Self and foreign continuum have opposite effects on longwave feedback at high surface temperatures
- Better understanding of continuum absorption is important to better constrain the temperature dependence of climate sensitivity

Correspondence to:
F. E. Roemer,
florian.roemer@uni-hamburg.de

Citation:
Roemer, F. E., Buehler, S. A., Kluft, L., & Pincus, R. (2024). Effect of uncertainty in water vapor continuum absorption on CO_2 forcing, longwave feedback, and climate sensitivity. *Journal of Advances in Modeling Earth Systems*, *16*, e2023MS004157. https://doi.org/10.1029/2023MS004157

Received 13 DEC 2023
Accepted 10 JUN 2024

Author Contributions:
Conceptualization: Florian E. Roemer, Stefan A. Buehler, Robert Pincus
Formal analysis: Florian E. Roemer
Funding acquisition: Robert Pincus
Investigation: Florian E. Roemer
Methodology: Florian E. Roemer, Stefan A. Buehler, Lukas Kluft
Project administration: Robert Pincus
Software: Florian E. Roemer, Lukas Kluft
Supervision: Stefan A. Buehler
Visualization: Florian E. Roemer
Writing – original draft: Florian E. Roemer
Writing – review & editing: Florian E. Roemer, Stefan A. Buehler, Lukas Kluft, Robert Pincus

Effect of Uncertainty in Water Vapor Continuum Absorption on CO_2 Forcing, Longwave Feedback, and Climate Sensitivity

Florian E. Roemer[1,2], Stefan A. Buehler[1], Lukas Kluft[3], and Robert Pincus[4]

[1]Center for Earth System Research and Sustainability (CEN), Meteorological Institute, Universität Hamburg, Hamburg, Germany, [2]International Max Planck Research School on Earth System Modelling (IMPRS-ESM), Hamburg, Germany, [3]Max Planck Institute for Meteorology, Hamburg, Germany, [4]Lamont-Doherty Earth Observatory, Columbia University, Palisades, NY, USA

Abstract We investigate the effect of uncertainty in water vapor continuum absorption at terrestrial wavenumbers on CO_2 forcing $\mathcal{F}$, longwave feedback λ, and climate sensitivity $\mathcal{S}$ at surface temperatures T_s between 270 and 330 K. We calculate this uncertainty using a line-by-line radiative-transfer model and a single-column atmospheric model, assuming a moist-adiabatic temperature lapse-rate and 80% relative humidity in the troposphere, an isothermal stratosphere, and clear skies. Due to the lack of a comprehensive model of continuum uncertainty, we represent continuum uncertainty in two different idealized approaches: In the first, we assume that the total continuum absorption is constrained at reference conditions; in the second, we assume that the total continuum absorption is constrained for all atmospheres in our model. In both approaches, we decrease the self continuum by 10% and adjust the foreign continuum accordingly. We find that continuum uncertainty mainly affects $\mathcal{S}$ through its effect on λ. In the first approach, continuum uncertainty mainly affects λ through a decrease in the total continuum absorption with T_s; in the second approach, continuum uncertainty affects λ through a vertical redistribution of continuum absorption. In both experiments, the effect of continuum uncertainty on $\mathcal{S}$ is modest at $T_s = 288$ K (≈0.02 K) but substantial at $T_s \geq 300$ K (up to 0.2 K), because at high T_s, the effects of decreasing the self continuum and increasing the foreign continuum have the same sign. These results highlight the importance of a correct partitioning between self and foreign continuum to accurately determine the temperature dependence of Earth's climate sensitivity.

Plain Language Summary Water vapor in Earth's atmosphere acts as a strong greenhouse gas by absorbing thermal radiation and thus plays a central role in controlling Earth's climate. Although water vapor absorption is well-understood overall, uncertainties remain in the so-called water vapor continuum, an absorption component that cannot yet be calculated from first principles. We investigate the impact of continuum uncertainty at terrestrial wavenumbers on climate sensitivity, the expected temperature increase that would result from a doubling of atmospheric CO_2 concentration. For this, we use a very simple climate model and represent continuum uncertainty in an idealized way. We find that uncertainty in the continuum mostly affects climate sensitivity by affecting the additional thermal radiation Earth emits to space as it warms. At temperatures similar to the current global average this effect is modest: changes in the water vapor continuum within the uncertainty only change climate sensitivity by 0.02 K, or about 1%. However, at temperatures similar to those in tropical regions, changes in the continuum within the uncertainty change climate sensitivity by up to 0.2 K, or about 6%. This shows that uncertainty in the water vapor continuum substantially contributes to uncertainty in the temperature dependence of climate sensitivity.

1. Introduction

Water vapor plays a central role in determining Earth's climate because it strongly absorbs and emits infrared radiation (Foote, 1856; Tyndall, 1861a, 1861b). Absorption by water vapor is well-understood overall but substantial uncertainty remains in the water vapor continuum, an absorption component that varies smoothly in the spectral dimension, and that is more uncertain than the line spectrum (e.g., Baranov et al., 2008; Ptashnik et al., 2011; Shine et al., 2012, 2016). Here we investigate the effect of this uncertainty at terrestrial wavenumbers on CO_2 forcing, longwave feedback, and climate sensitivity.

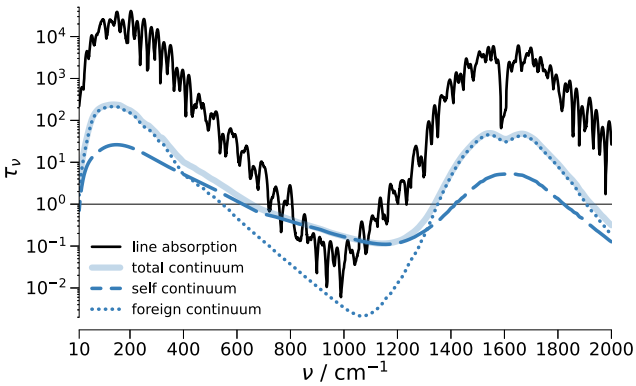

Figure 1. Importance of water vapor continuum strongly varies spectrally. Shown are the spectrally resolved opacities τ_ν of water vapor as a function of wavenumber ν (20 cm^{-1} moving average) for an atmospheric column (288 K surface temperature, 80% relative humidity). Shown are the τ_ν of water vapor lines (black), total water vapor continuum (light blue), as well as split into water vapor self continuum (dashed blue) and water vapor foreign continuum (dotted blue).

Uncertainty in the water vapor continuum fundamentally arises from uncertainty in the underlying physical processes. Possible explanations for the continuum discussed in the literature include far-wing absorption of single water vapor molecules (e.g., Clough et al., 1989; Ma & Tipping, 1991), absorption by bound and quasi-bound complexes of two water vapor molecules (e.g., Mukhopadhyay et al., 2015; Ptashnik et al., 2011) and of water and non-water molecules such as nitrogen or oxygen (e.g., Vigasin, 2000), as well as collision-induced absorption (e.g., Baranov & Lafferty, 2012). Although it seems likely that no single process is sufficient to explain the continuum, substantial uncertainty remains regarding the relative importance of these processes (e.g., Mlawer et al., 2023; Shine et al., 2012, 2016).

Therefore, continuum absorption cannot yet be calculated from first principles but is rather estimated using semi-empirical continuum models, most commonly the Mlawer-Tobin-Clough-Kneizys-Davies model (MT_CKD, Mlawer et al., 2023). This is commonly done by—somewhat arbitrarily—truncating water vapor absorption lines at 25 cm^{-1} from the line center; the remaining water vapor absorption is then defined as continuum absorption (e.g., Clough et al., 1989; Mlawer et al., 2023; Shine et al., 2012; Tipping & Ma, 1995). This continuum absorption is further split into two components: (a) The self continuum comprises absorption due to interactions between two water molecules and thus depends quadratically on water vapor volume mixing ratio q; furthermore, self continuum absorption decreases with temperature T. (b) The foreign continuum comprises absorption due to interactions between a water molecule and a non-water molecule and thus depends linearly on q, with no known dependence on T (e.g., Burch & Alt, 1984; Mlawer et al., 2023; Shine et al., 2016).

To accurately determine the water vapor continuum and its components, models rely on data from laboratory measurements (e.g., Fournier et al., 2024; Odintsova et al., 2022; Paynter et al., 2009), satellite observations (e.g., Newman et al., 2012), and field campaigns (e.g., Liuzzi et al., 2014; Serio et al., 2008). However, those measurements still exhibit both substantial spread and spectral gaps which further contribute to uncertainty (Baranov et al., 2008; Ptashnik et al., 2011; Shine et al., 2016). This uncertainty concerns both the absorption of solar radiation in the visible and near-infrared spectral ranges as well as the absorption of terrestrial radiation in the mid- and far-infrared spectral ranges (Shine et al., 2016). In this study, we exclusively focus on the effect of the continuum on terrestrial radiation.

Continuum absorption is strongest within water vapor absorption bands but its climate impact is strongest in the atmospheric windows where the self continuum is often the dominant absorber (Figure 1). In the context of terrestrial radiation, the mid-infrared window (750 cm^{-1} to 1,250 cm^{-1}) is particularly relevant because a substantial part of the outgoing longwave radiation $\mathcal{L}$ is emitted here.

As surface temperature T_s increases—and relative humidity stays constant—q increases exponentially. This increase in q causes both self and foreign continuum absorption to strongly increase with T_s, more than offsetting the self continuum's negative direct dependence on T (Pierrehumbert, 2010). At $T_s \approx 300$ K continuum absorption becomes optically thick which closes the mid-infrared window and strongly inhibits Earth's ability to radiate energy to space (e.g., Koll & Cronin, 2018). This directly affects Earth's longwave feedback λ, the change in $\mathcal{L}$ with T_s. Furthermore, both self and foreign continuum mask part of the absorption by CO_2 and thus reduce the magnitude of CO_2 forcing $\mathcal{F}$ (Jeevanjee, Seeley, et al., 2021). Consequently, continuum absorption directly affects climate sensitivity $\mathcal{S} = -\mathcal{F}/\lambda$, the temperature increase caused by a CO_2 doubling (e.g., Stevens & Kluft, 2023).

At the same time, uncertainty in self continuum absorption in the mid-infrared window is still around 10%–20% and does not seem to decrease over time (see Figure 2, also e.g., Baranov et al., 2008; Shine et al., 2016). In many cases, uncertainty is even larger for the foreign continuum and within water vapor bands because measurements there are impeded by the very strong line absorption (Paynter & Ramaswamy, 2011, 2012). Furthermore, uncertainties in self and foreign continuum are usually correlated (see Section 4, also e.g., Shine et al., 2016).

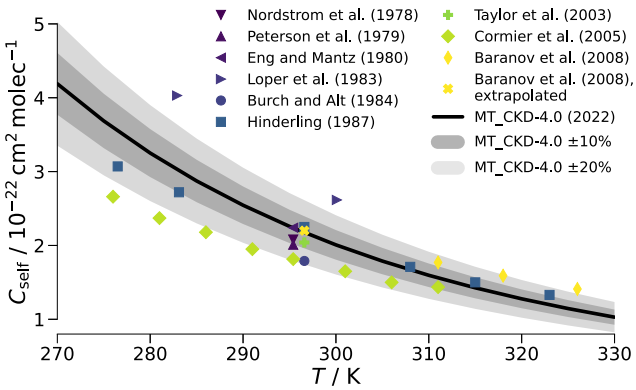

Figure 2. Water vapor continuum absorption is still uncertain. As an example, the self continuum absorption cross-section C_{self} at 944.19 cm^{-1} is shown as function of temperature T from MT_CKD version 4.0 (Mlawer et al., 2023) (line) and from laboratory measurements (symbols). The shaded areas correspond to differences of ±10% and ±20% from MT_CKD, respectively. The measurements at 296 K are slightly offset along the temperature axis for better visibility. Laboratory data were read off from Baranov et al. (2008, their Figure 8) and Ptashnik et al. (2011, their Figure 7). (Eng & Mantz, 1980; Hinderling et al., 1987; Loper et al., 1983; Nordstrom et al., 1978; Peterson et al., 1979; Taylor et al., 2003).

Given the direct effect of continuum absorption on $\mathcal{F}$ and λ, this substantial uncertainty raises two important questions: (a) How large is the resulting uncertainty in $\mathcal{F}$ and λ—and thus $\mathcal{S}$—in the context of contemporary climate change? (b) How does this uncertainty affect the surface temperature dependence of these quantities (e.g., Kluft et al., 2021; Meraner et al., 2013; Romps, 2020; Seeley & Jeevanjee, 2021)? These surface temperature dependences can be helpful to investigate $\mathcal{F}$, λ, and $\mathcal{S}$ in past climates of Earth where the global-mean surface temperature was substantially lower or higher than it is today, but also to analyze how $\mathcal{F}$ and λ vary throughout different climate zones on present-day Earth.

To date, uncertainty in water vapor continuum absorption has mostly been discussed within the field of spectroscopy (e.g., Baranov et al., 2008; Ptashnik et al., 2011; Shine et al., 2012, 2016). In the climate community, the importance of the water vapor continuum for λ is well-established (e.g., Koll et al., 2023; Seeley & Jeevanjee, 2021; Stevens & Kluft, 2023), but much less is known about how uncertainty in the continuum propagates to uncertainty in $\mathcal{L}$, $\mathcal{F}$, and λ (Kiehl & Ramanathan, 1982; Paynter & Ramaswamy, 2011, 2012), and how it affects $\mathcal{S}$.

To expand on those studies, we take a holistic look at the effect of uncertainty in water vapor continuum absorption at terrestrial wavenumbers on $\mathcal{F}$, λ and $\mathcal{S}$, as well as their temperature dependences, using an idealized atmospheric model. To this end, we first develop a conceptual understanding of how independent variations in self and foreign continuum absorption differently affect $\mathcal{F}$, λ, and $\mathcal{S}$ (Section 3). We then investigate the effect of continuum uncertainty. Given the lack of a comprehensive model of continuum uncertainty, we represent this uncertainty using two different idealized approaches (Section 4). Throughout, we illuminate the underlying processes by spectrally decomposing the effect of continuum uncertainty on $\mathcal{F}$ and λ, bridging the gap between spectroscopy and climate science.

2. Methods

2.1. Atmospheric Model

We use the single-column model konrad (Dacie et al., 2019; Kluft et al., 2019) to create profiles of temperature $\boldsymbol{T}$ and water vapor volume mixing ratio $\boldsymbol{q}$ on 256 vertical levels for surface temperatures $T_s \in [269\ \text{K}, 331\ \text{K}]$ in 1 K increments. The $\boldsymbol{T}$ profiles follow a moist adiabat in the troposphere until they reach 175 K. Above, we assume a fixed isothermal stratosphere with $\boldsymbol{T} = 175$ K. This approach eliminates stratospheric feedbacks and allows us to focus exclusively on the troposphere.

Relative humidity is set to 80% in the troposphere and stratospheric $\boldsymbol{q}$ is set to the tropopause value. The effect of this simplified assumption is discussed in Section 5.1. The concentrations of trace gases follow the convention of the Aqua-Planet Experiment also used in the Radiative-convective equilibrium model intercomparison project (Wing et al., 2018): 348 ppm CO_2, 1,650 ppb CH_4, and 306 ppb N_2O. The O_3 concentration follows the profile derived by Wing et al. (2018), which is a function of pressure only and does not account for changes caused by the vertical expansion of the troposphere with T_s. However, this approach captures the first-order effect of ozone, namely the masking of emission in the window.

2.2. Radiative Transfer Model

For each T_s we calculate the spectrum of clear-sky outgoing longwave radiation $\mathcal{L}_\nu$ using the line-by-line radiative transfer model ARTS (Buehler et al., 2018; Eriksson et al., 2011). We perform the calculations at 32,768 (2^{15}) frequencies uniformly spanning the spectral range 10 cm^{-1} to 3,250 cm^{-1}, accounting for absorption by water vapor, CO_2, CH_4, N_2O, O_3, N_2 and O_2.

Line absorption in ARTS is calculated using the internal ARTS Catalog Data, which in turn is based on the high-resolution transmission molecular absorption database (HITRAN, Gordon et al., 2022) as of 2022–05–02. Continuum absorption is calculated using the latest (at the time of analysis) MT_CKD models for CO_2 and N_2

(both version 2.5), O_2 (version 1.0), as well as water vapor (version 4.0), which has also been included in both HITRAN and the ARTS Catalog Data (Mlawer et al., 2023). At the time of writing, the only changes made since concern minor revisions of the water vapor foreign continuum in version 4.1.1 (Mlawer et al., 2023). Consistent with MT_CKD, water vapor lines are cut off at 25 cm^{-1} from the line center. Wings beyond that wavenumber and the associated "pedestal" under the line are removed, as described in detail in Clough et al. (1989).

2.3. CO_2 Forcing, Longwave Feedback, and Climate Sensitivity

For each T_s we calculate the spectrally resolved clear-sky 2 × CO_2 radiative forcing $\mathcal{F}_\nu$ by performing simulations of spectrally resolved clear-sky outgoing longwave radiation $\mathcal{L}_\nu$ at two different CO_2 concentrations: a baseline concentration of 348 ppm (note that this differs from the often-used pre-industrial value of 280 ppm) and a doubled CO_2 concentration of 696 ppm. The clear-sky spectral CO_2 forcing is then

$$\mathcal{F}_\nu(T_s) = -[\mathcal{L}_\nu(T_s, 696\ \text{ppm}\ CO_2) - \mathcal{L}_\nu(T_s, 348\ \text{ppm}\ CO_2)]. \tag{1}$$

Here $\mathcal{F}_\nu$ is the instantaneous radiative forcing, as our experimental setup does not allow for stratospheric cooling and the resulting radiative adjustment. However, as the stratosphere contains so little water vapor, the continuum presumably has no impact on the adjustment process, and thus continuum uncertainty is expected to have the same effect on instantaneous forcing as it would on effective forcing, the relevant quantity for calculating climate sensitivity.

For each T_s we calculate the spectrally resolved clear-sky longwave feedback λ_ν as the centered finite difference

$$\lambda_\nu(T_s) = -\frac{\mathcal{L}_\nu(T_s + 1\ \text{K}, \boldsymbol{T}_{i+1}, \boldsymbol{q}_{i+1}) - \mathcal{L}_\nu(T_s - 1\ \text{K}, \boldsymbol{T}_{i-1}, \boldsymbol{q}_{i-1})}{2\ \text{K}}, \tag{2}$$

where $\boldsymbol{x}_{i\pm1} = \boldsymbol{x}\ (T_s \pm 1\ \text{K})$ for the profiles of temperature $\boldsymbol{T}$ and water vapor volume mixing ratio $\boldsymbol{q}$, respectively.

The spectral surface feedback $\lambda_{\nu,\,\text{sfc}}$ is defined as the change in $\mathcal{L}_\nu$ that is caused by variations in T_s alone, with $\boldsymbol{T}$ and $\boldsymbol{q}$ unchanged. Therefore, we calculate it as

$$\lambda_{\nu,\,\text{sfc}}(T_s) = -\frac{\mathcal{L}_\nu(T_s + 1\ \text{K}, \boldsymbol{T}_i, \boldsymbol{q}_i) - \mathcal{L}_\nu(T_s - 1\ \text{K}, \boldsymbol{T}_i, \boldsymbol{q}_i)}{2\ \text{K}}, \tag{3}$$

where $\boldsymbol{x}_i = \boldsymbol{x}\ (T_s)$ for $\boldsymbol{x} \in \{\boldsymbol{T}, \boldsymbol{q}\}$.

The spectral atmospheric feedback, the radiative signature of changes in $\boldsymbol{T}$ and $\boldsymbol{q}$, is calculated as

$$\lambda_{\nu,\,\text{atm}}(T_s) = \lambda_\nu(T_s) - \lambda_{\nu,\,\text{sfc}}(T_s). \tag{4}$$

These spectrally resolved quantities are integrated to yield the broadband quantities as

$$a(T_s) = \int_{\nu_0}^{\nu_1} a_\nu(T_s)\ \mathrm{d}\nu, \tag{5}$$

where $a \in \{\mathcal{F}, \lambda, \lambda_{\text{sfc}}, \lambda_{\text{atm}}\}$ and $(\nu_0, \nu_1) = (10\ cm^{-1}, 3{,}250\ cm^{-1})$.

Finally, the longwave clear-sky climate sensitivity $\mathcal{S}$, the temperature increase caused by a CO_2 doubling assuming clear skies and constant albedo, is calculated as

$$\mathcal{S}(T_s) = -\frac{\mathcal{F}(T_s)}{\lambda(T_s)}. \tag{6}$$

2.4. Emission Fraction

To analyze the different impacts of self and foreign continuum on λ_ν, we calculate the emission fraction f_{em} which represents which species dominates different spectral regions at different surface temperatures T_s. To this end, we

calculate the spectrally resolved opacity $\tau_{\nu,s}(p)$ of each absorbing species s from the top of the atmosphere (TOA) to each pressure level p using ARTS. In addition to CO_2 and water vapor lines, we consider the self and foreign continuum separately.

The emission pressure $p_{\mathrm{em},\nu,s}$ of each species is then defined as the largest p, that is, the lowest level, where $\tau_{\nu,s}(p) \leq 1$ as seen from TOA. From this, we define the "emitting" species at each wavenumber ν as the species with the smallest $p_{\mathrm{em},\nu,s}$, that is, the species that emits from the highest level in the atmosphere. If no species has $\tau_{\nu,s} > 0.5$ at the surface, we neglect atmospheric emission and no "emitting" species is chosen for that wavenumber; if multiple species have the same $p_{\mathrm{em},\nu,s}$, they all contribute to atmospheric emission so all of them are chosen as "emitting" species.

We separately consider three main spectral regions of interest: the FIR water vapor band (FIR, 200 cm^{-1} to 600 cm^{-1}), the major CO_2 band (600 cm^{-1} to 750 cm^{-1}), and the atmospheric window (750 cm^{-1} to 1,250 cm^{-1}). We define the emission fraction $f_{\mathrm{em},s}$ (T_s) as the fraction of all simulated wavenumbers within each of those spectral regions at which each species s is the "emitting" species, estimating which species most strongly impacts atmospheric emission and thus λ at a given T_s.

2.5. Uncertainty in Continuum Absorption

We perform a number of different experiments in which we vary the magintude of the water vapor continuum. Apart from the baseline experiment with the unaltered continuum, we separately vary the magnitude of self and foreign continuum by ±10%. Finally, we perfrom two different experiments to represent continuum uncertainty in an idealized way. Both of them are based on the assumption that the total continuum absorption is well-constrained, and that the main uncertainty arises from the partitioning between self and foreign continuum. In the single-constraint experiment, we assume that the constraint on the total continuum applies at a single set of reference conditions, while in the general-constraint experiment, we assume that the constraint generally applies at all atmospheric conditions. In the following, these two experiments are described in more detail.

2.5.1. The Single-Constraint Experiment

We assume that the spectrally resolved total continuum opacity $\tau_{\nu,\mathrm{cont}}$ is perfectly constrained for reference values of temperature $T_0 = 296$ K, air pressure $p_0 = 1013$ hPa, and water vapor volume mixing ratio $q_0 = 0.02$. These values are chosen to mimic conditions commonly present in both laboratory and field studies of the continuum, which provide a constraint on the total continuum absorption. For a discussion about the effect of the choice of q_0 see Section 5.2.

We assume a spectrally uniform uncertainty in the self continuum of ±10%, and account for the negative correlation between self and foreign continuum uncertainty by adjusting the foreign continuum accordingly. We derive this adjustment from the reference opacities $\tau_{\nu,\mathrm{self},0} = \tau_{\nu,\mathrm{self}}(T_0, p_0, q_0)$ and $\tau_{\nu,\mathrm{foreign},0} = \tau_{\nu,\mathrm{foreign}}(T_0, p_0, q_0)$. The scaling factor x_ν is then defined as the factor $\tau_{\nu,\mathrm{foreign},0}$ has to be multiplied with to compensate for a change in $\tau_{\nu,\mathrm{self},0}$ of ±10% so that the total continuum opacity at the given reference values is conserved. This yields

$$x_\nu^{\pm} = 1 \mp 0.1 \cdot \frac{\tau_{\nu,\mathrm{self},0}}{\tau_{\nu,\mathrm{foreign},0}}, \tag{7}$$

where x_ν^+ is the scaling factor for the foreign continuum if the self continuum is increased by +10% and vice versa.

This adjustment of the foreign continuum is only of $\mathcal{O}(10\%)$ in the water vapor bands, but exceeds 100% in the atmospheric windows, where the self continuum is much stronger than the foreign continuum. This large adjustment in the windows means that an increase of the self continuum by 10% would cause the new self continuum to be stronger than the current total continuum—and thus would require negative foreign continuum absorption to achieve radiative closure in the case of x_ν^+. This indicates that a substantially stronger self continuum is unlikely, at least in the windows. This is also consistent with the fact that more recent laboratory studies based on cavity ring down spectroscopy observe weaker self continuum absorption in the 1,000 cm^{-1} window than

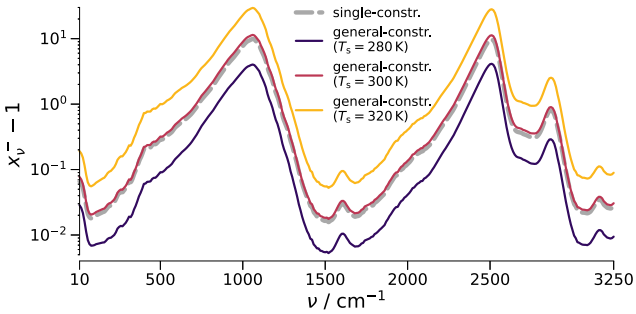

Figure 3. Scaling factors x_ν^- for foreign continuum to compensate for change in self continuum of −10%. Shown are the x_ν^- for the single-constraint experiment (dashed) and the $x_\nu^-(T_s)$ general-constraint experiment for selected surface temperatures T_s (solid).

predicted by MT_CKD 4.0 (Cormier et al., 2005; Fournier et al., 2024). Therefore, we only focus on the case where the self continuum is decreased by 10% and the foreign continuum is increased by factor x_ν^-.

2.5.2. The General-Constraint Experiment

We assume that the spectrally resolved column-integrated total continuum opacity $\tau_{\nu,\,\mathrm{cont}}$ is perfectly constrained for all of our atmospheric profiles. This means that we derive the foreign continuum scaling factor x_ν separately for each T_s, using the temperature and humidity profiles described in Section 2.1. We calculate $\tau_{\nu,\mathrm{self}}(T_s) = \tau_{\nu,\mathrm{self}}(\boldsymbol{T}_i, \boldsymbol{p}_i, \boldsymbol{q}_i)$ and $\tau_{\nu,\mathrm{foreign}}(T_s) = \tau_{\nu,\mathrm{foreign}}(\boldsymbol{T}_i, \boldsymbol{p}_i, \boldsymbol{q}_i)$, where $\boldsymbol{x}_i = \boldsymbol{x}(T_s)$ for $\boldsymbol{x} \in \{\boldsymbol{T}, \boldsymbol{p}, \boldsymbol{q}\}$. From this, we analogously derive the scaling factor

$$x_\nu^-(T_s) = 1 + 0.1 \cdot \frac{\tau_{\nu,\mathrm{self}}(T_s)}{\tau_{\nu,\mathrm{foreign}}(T_s)}, \tag{8}$$

where, for the same reasons described above, we only consider the case of a 10% decrease in the self continuum and an increase in the foreign continuum by factor $x_\nu^-(T_s)$. Because the self continuum increases much more strongly with T_s than the foreign continuum, the adjustment of the foreign continuum strongly increases with T_s (Figure 3).

3. Effect of Variations in Self and Foreign Continuum

Before we proceed to investigate the impact of overall continuum uncertainty, this section first investigates the effect of variations in self and foreign continuum absorption in order to understand the relevant physical mechanisms. To this end, we separately vary the magnitude of self and foreign continuum absorption by ±10% throughout the whole simulated spectral range (10 cm^{-1} to 3,250 cm^{-1}). This way, we investigate how self and foreign continuum differently affect both CO_2 forcing and longwave feedback.

3.1. Effect on CO_2 Forcing

Conceptually, the clear-sky CO_2 forcing $\mathcal{F}$ depends on two factors (Jeevanjee, Seeley, et al., 2021). First, the temperature contrast between surface and stratosphere determines $\mathcal{F}$ in a dry atmosphere because surface emission is replaced with stratospheric emission at the edges of CO_2 absorption bands. Second, the presence of water vapor means that part of the original emission originates from the troposphere rather than the surface, due both water vapor line and continuum absorption. This change in the original emission level reduces the temperature contrast with the stratosphere and thus weakens $\mathcal{F}$.

At low T_s the spectrally resolved forcing $\mathcal{F}_\nu$ is most pronounced at the edges of the major CO_2 band (600 cm^{-1} to 750 cm^{-1}). At high T_s—and thus large water vapor volume mixing ratios $\boldsymbol{q}$—water vapor absorption masks $\mathcal{F}_\nu$ at the CO_2 band edges, while the concomitant vertical expansion of the troposphere "unlocks" a substantial $\mathcal{F}_\nu$ in the CO_2 band center (Jeevanjee, Seeley, et al., 2021; Kluft et al., 2021; Seeley & Jeevanjee, 2021, see also Figure 4a). Overall, $\mathcal{F}$ increases with T_s until around 295 K due to the increasing surface-stratosphere temperature contrast; at even higher T_s the weakening effect of the exponentially increasing $\boldsymbol{q}$ dominates (Kluft et al., 2021, see also Figure 5a). For the minor CO_2 bands in the atmospheric window around 950 cm^{-1} and 1,050 cm^{-1} this decrease in $\mathcal{F}$ is roughly uniform, while for the major CO_2 band at 667 cm^{-1} $\mathcal{F}$ decreases slowly at first and much more strongly above $T_s \approx 315$ K (see Figure 5a).

Together with water vapor line absorption, the water vapor continuum determines the atmospheric layer whose emission is replaced by stratospheric emission when CO_2 is doubled. When continuum absorption is increased, the original emission level is located at lower temperatures. Hence, the temperature contrast with the stratosphere is smaller which weakens $\mathcal{F}$, and vice versa for a decreased continuum. Consequently, the effect of the continuum on $\mathcal{F}_\nu$ is mostly limited to the edges of the CO_2 absorption bands (Figures 4e and 4i).

Due to the exponential Clausius-Clapeyron relation and the quadratic dependence of the self continuum on $\boldsymbol{q}$, the effect of the self continuum on $\mathcal{F}$ increases with T_s until around 310 K and stays constant for even higher T_s

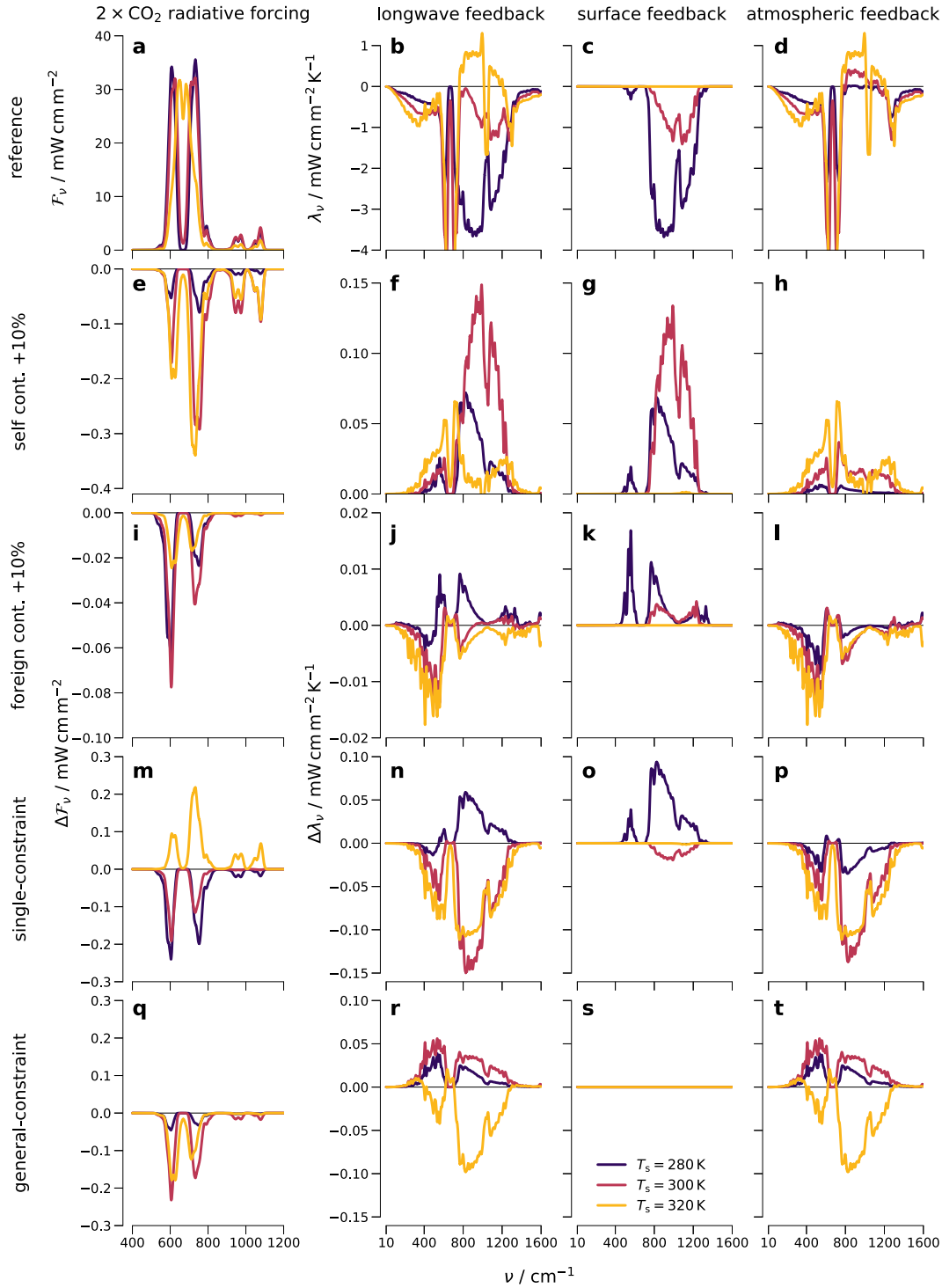

Figure 4. Spectrally-resolved effect of water vapor continuum absorption on CO_2 forcing $\mathcal{F}_\nu$ (a, e, i, m) and longwave feedback λ_ν (b, f, j, n), which is also decomposed into surface feedback (c, g, k, o) and atmospheric feedback (d, h, l, p) for surface temperatures T_s of 280 K (black), 300 K (red), and 320 K (yellow). Shown are the baseline values (a–d), and the effects of 10% increase in self continuum absorption (e–h) and foreign continuum absorption (i–l). Finally, the results are shown for the single-constraint (m–p) and general-constraint experiments (q–t).

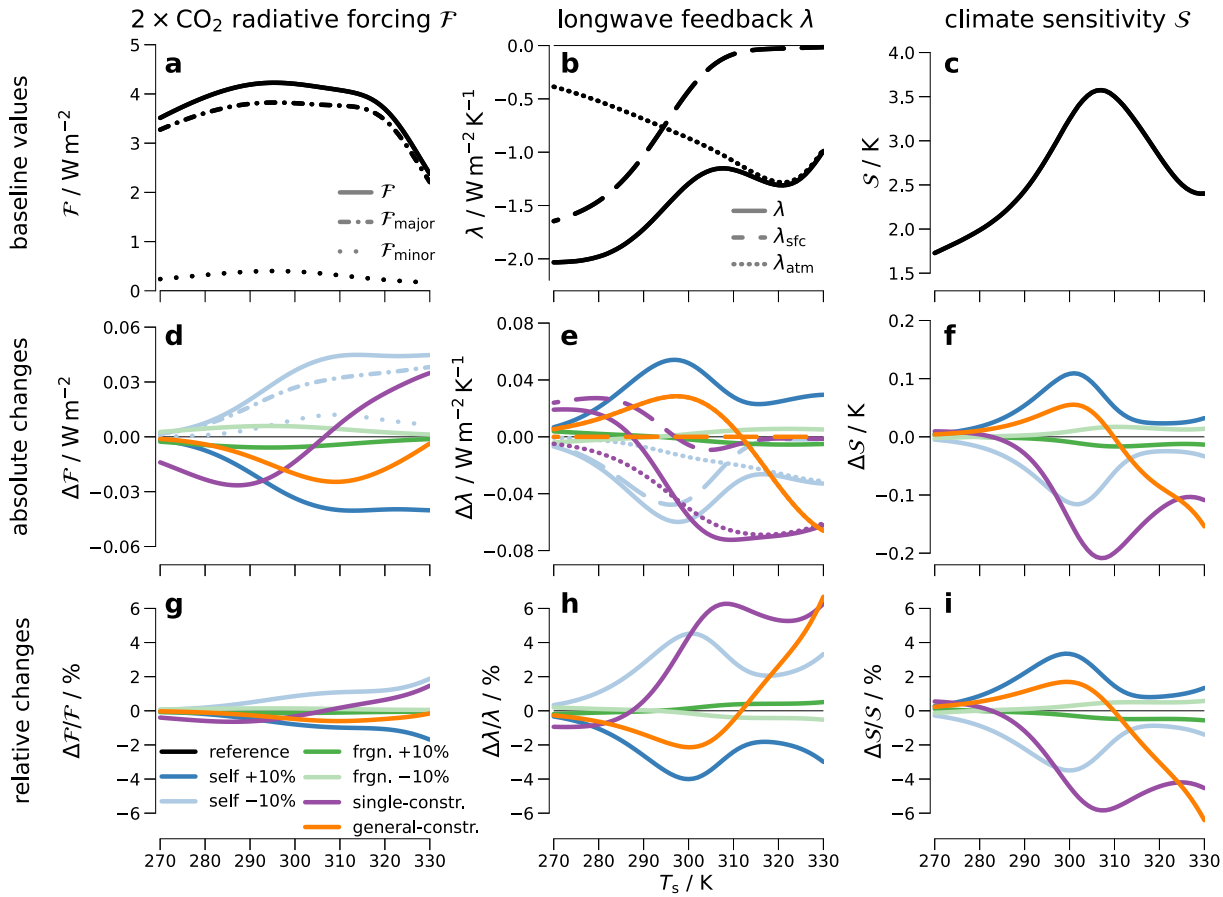

Figure 5. Spectrally-integrated effect of water vapor continuum on CO_2 forcing $\mathcal{F}$ (a, d, g), longwave feedback λ (b, e, h), and climate sensitivity $\mathcal{S}$ (c, f, i). Shown are the total values (a–c) of the baseline simulation (black), as well as the absolute differences Δx (d–f) and relative differences $\frac{\Delta x}{x}$ (g–i) caused by variations in self continuum (blue) and foreign continuum (green) of +10% (dark shading) and −10% (light shading) for $x \in \{\mathcal{F}, \lambda, \mathcal{S}\}$. The same quantities are shown for the single-constraint experiment (purple), as well as for the general-constraint experiment (orange). For selected experiments, the forcing terms are split into the contribution by the major CO_2 band $\mathcal{F}_{\text{major}}$ ($\nu < 900\ \text{cm}^{-1}$, dash-dotted) and minor CO_2 bands $\mathcal{F}_{\text{minor}}$ ($\nu > 900\ \text{cm}^{-1}$, loosely dotted), and the feedback terms are split into surface feedback λ_{sfc} (dashed) and atmospheric feedback λ_{atm} (dotted).

(Figures 5d and 5g). This results from compensation between the self continuum's effect on the forcing contributions of the major CO_2 band and the minor CO_2 bands. The effect of the self continuum on the forcing contribution of the minor CO_2 bands decreases above 310 K because self continuum absorption becomes much stronger than CO_2 absorption in the window. This in turn is because CO_2 concentration stays constant with T_s in our experiments, while $\boldsymbol{q}$ increases exponentially. In contrast, the effect of the self continuum on the forcing contribution of the much stronger major CO_2 band continues to increase with T_s (Figures 5d and 5g).

For the same perturbation of ±10%, the foreign continuum has a much weaker effect on $\mathcal{F}$. Because it is much weaker in the atmospheric window than the self continuum, the foreign continuum only affects the major CO_2 band and mainly at $T_s \leq 310$ K (Figures 4i and 5d).

For $T_s = 288$ K, the spectrally integrated effect of both water vapor self and foreign continuum on $\mathcal{F}$ is small: variations of ±10% in the self continuum only change $\mathcal{F}$ by less than 0.02 W m^{-2} (0.4%), the same variations in the foreign continuum have an even smaller effect of <0.01 W m^{-2} (0.1%). Even at $T_s = 320$ K variations in the self continuum only change $\mathcal{F}$ by around 0.04 W m^{-2} (1%). These uncertainties are smaller than those found by Paynter and Ramaswamy (2012), who assumed a larger, spectrally varying uncertainty in the continuum of up to ±50% and consequently found an uncertainty in $\mathcal{F}$ of up to ±3% (their Figure 14).

3.2. Effect on Longwave Feedback

Before we analyze the effect of variations in the water vapor self and foreign continuum on the longwave feedback λ, we briefly review the current understanding of its spectrally resolved counterpart λ_ν (Figure 4b). In the atmospheric window (750 cm^{-1} to 1,250 cm^{-1}), λ_ν is mostly governed by the strongly stabilizing (negative) surface feedback λ_{sfc}. However, the window continuously closes with increasing T_s which weakens λ_{sfc} and causes it to almost vanish at $T_s \approx 310$ K (e.g., Koll & Cronin, 2018; Kluft et al., 2021, see also Figures 4c and 5b). Above 310 K the dependence of λ_ν in the window on water vapor volume mixing ratio $\boldsymbol{q}$ and thus on T_s is weaker than at lower T_s. This is because λ_{sfc} is replaced by a weakly destabilizing (positive) atmospheric feedback λ_{atm} caused by the water vapor continuum which is described in more detail below (Koll et al., 2023, see also Figures 4d and 5b). This atmospheric feedback is less senstitive to changes in T_s than λ_{sfc} is during the closing of the window, and thus the total feedback λ is less sensitive to T_s above 310 K.

Outside the window region, λ_ν is almost entirely determined by λ_{atm}. In the center of the major CO_2 band (600 cm^{-1} to 750 cm^{-1}), λ_{atm} is close to zero at $T_s = 288$ K because the emission level there is located in the stratosphere but becomes strongly stabilizing at high T_s due to the vertical expansion of the troposphere. This stabilizing λ_{atm} is strongest at the band edges, where it is already present for $T_s < 288$ K, but also reaches the band center at $T_s > 300$ K. At $T_s > 320$ K the stabilizing λ_{atm} is weakened due to masking by water vapor absorption (Kluft et al., 2021; Seeley & Jeevanjee, 2021, see also Figures 4d and 5b).

Finally, λ_{atm} is weakly stabilizing in the water vapor bands in the far-infrared (FIR, 200 cm^{-1} to 600 cm^{-1}) and mid-infrared (MIR, 1,250 cm^{-1} to 2,000 cm^{-1}), which are dominated by water vapor line absorption. Here, the first-order approximation of a constant emission temperature would imply constant $\mathcal{L}$ with T_s—and thus a neutral λ_{atm} assuming $\tau \gg 1$ (Ingram, 2010; Jeevanjee, Koll, & Lutsko, 2021; Simpson, 1928a, 1928b). However, this approximation does not hold entirely due to effects like pressure broadening which induce a weakly stabilizing λ_{atm} (Feng et al., 2023; Koll et al., 2023, see also Figure 4d).

Water vapor continuum absorption affects λ by altering both λ_{sfc} and λ_{atm} (Koll et al., 2023). In the following, we therefore discuss the partial feedbacks induced by separately increasing self and foreign continuum by 10%. A destabilizing partial feedback means that the total feedback becomes less stabilizing, and vice versa.

The continuum dampens the stabilizing λ_{sfc} in the atmospheric window by damping surface emission. Hence, a stronger continuum dampens λ_{sfc} more and thus induces a destabilizing partial feedback at $T_s < 310$ K, when the window is still open, and vice versa for a weaker continuum. This destabilizing partial feedback can be seen for both continuum components, but the effect of the self continuum (Figure 4g) is much stronger than that of the foreign continuum (Figure 4k) for the same perturbation of +10%.

The continuum affects λ_{atm} because its emission temperature is sensitive to the temperature lapse rate. Because the moist-adiabatic lapse rate decreases with warming this leads to an additional increase in $\boldsymbol{q}$. This in turn causes the continuum to emit at lower temperatures, giving rise to a destabilizing lapse-rate feedback (Koll et al., 2023). The effect of variations in the self continuum on λ_{atm} is weaker than that on λ_{sfc} below $T_s \approx 310$ K but becomes the dominant effect at higher T_s (Figure 5e). Below $T_s \approx 300$ K the effect on λ_{atm} is mostly limited to the atmospheric window but it also reaches the absorption bands of water vapor and CO_2 at higher T_s. This destabilizing effect of an increased self continuum on λ_{atm} continuously increases with T_s in both water vapor and CO_2 absorption bands, while in the window it peaks at around 300 K and slowly decreases at higher T_s (Figure 4h). In contrast, the foreign continuum has a weakly stabilizing effect on λ_{atm} throughout the spectrum, particularly in the FIR water vapor band (Figure 4l).

The stabilizing effect of a foreign continuum increase might seem surprising at first. To understand it, and also the other described changes, it is useful to think of them as resulting from shifts in the absorption species that control the main spectral regions as T_s increases. These shifts can be seen by looking at the emission fraction $f_{em,\,s}\,(T_s)$, which quantifies how much of the emission in a certain spectral band is controlled by species s at surface temperature T_s (see Section 2.4 for details). This approach allows us to explain (a) differences between self and foreign continuum, (b) differences among spectral regions, and (c) dependence on surface temperature T_s (Figure 6). The explanation relies on the dependences of the opacity of the different absorbing species on $\boldsymbol{q}$ and thus on T_s under constant relative humidity (Figure 6 first column) which can be expressed as

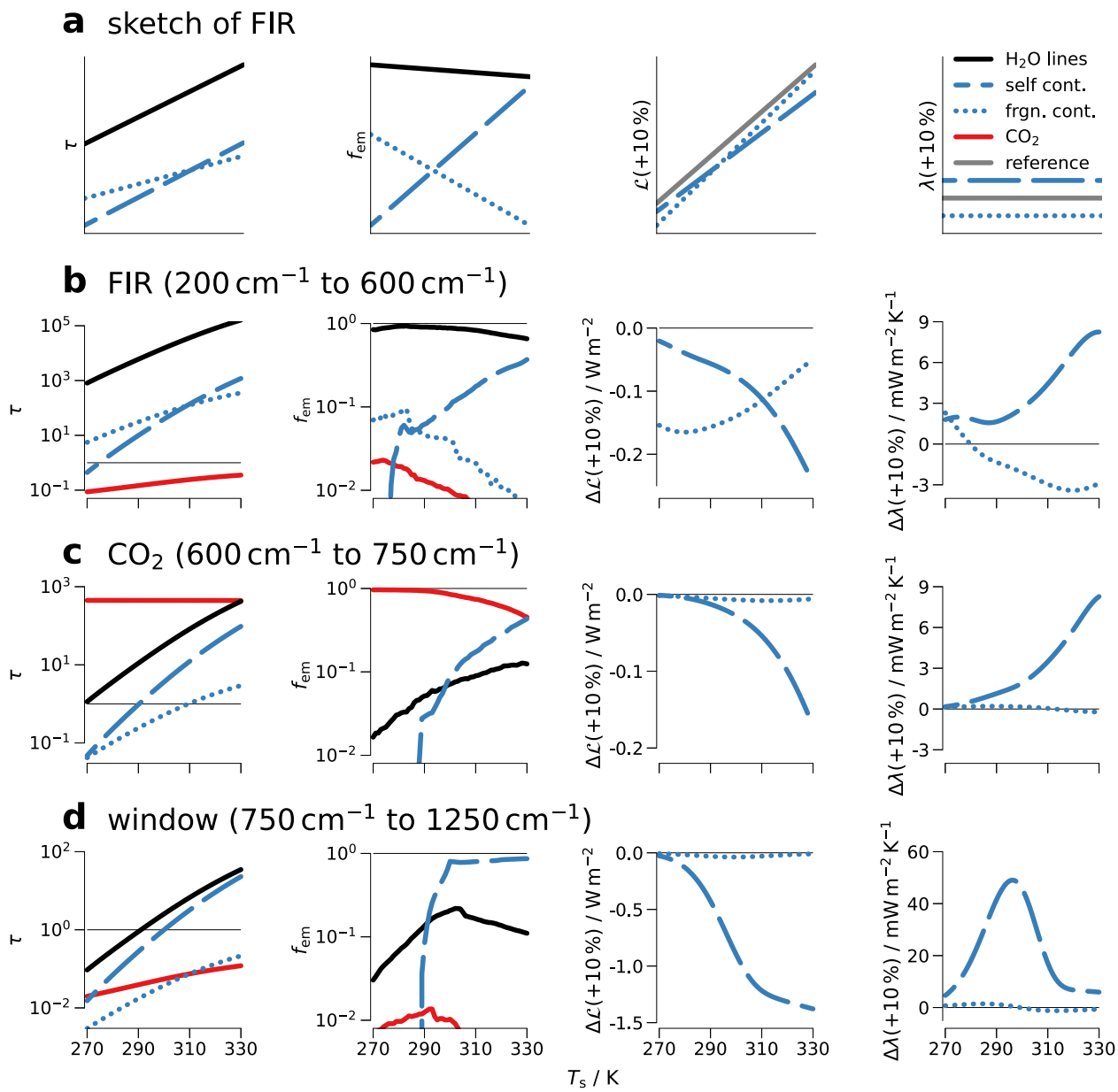

Figure 6. Absorption species that control the different spectral regions shift with surface temperature T_s. Shown are band-averaged opacity τ (first column), band emission fraction f_{em} (second column), band-integrated outgoing longwave radiation $\mathcal{L}$ (third column), and band-integrated longwave feedback λ (fourth column). An idealized sketch of the mechanism in the far-infrared (FIR) water vapor absorption band is shown in the first row. Below, the actual values are shown for the FIR band, the major CO_2 band, and the atmospheric window. Note that the results shown in the third and fourth columns represent the changes in $\mathcal{L}$ and λ caused by increasing self and foreign continuum absorption by 10%, except for the first row where the absolute values of $\mathcal{L}$ and λ are sketched.

$$\frac{\mathrm{dlog}(\tau_{\mathrm{self}})}{\mathrm{d}T_s} > \frac{\mathrm{dlog}(\tau_{\mathrm{H_2O\ lines}})}{\mathrm{d}T_s} > \frac{\mathrm{dlog}(\tau_{\mathrm{foreign}})}{\mathrm{d}T_s} > \frac{\mathrm{dlog}(\tau_{\mathrm{CO_2}})}{\mathrm{d}T_s}. \tag{9}$$

Regarding the opposite signs of the partial feedbacks of self and foreign continuum, the implications of Equation 9 are sketched for the FIR water vapor band (Figure 6a). This sketch also builds on results of the radiative transfer simulations shown in Figure 6b. The strong T_s dependence of τ_{self} means that the self continuum "gains ground" compared to the other species and thus $f_{\mathrm{em,self}}$ strongly increases with T_s. In contrast, the weak T_s dependence of τ_{foreign} means that the foreign continuum "loses ground" compared to the other species and thus

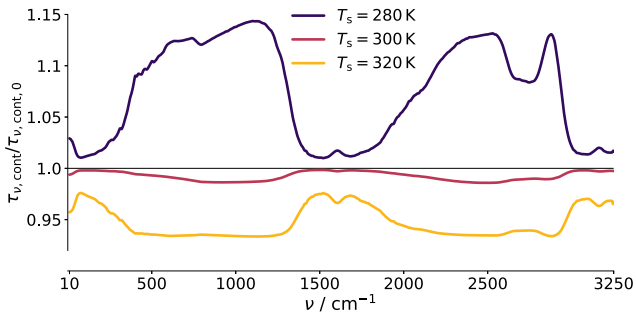

Figure 7. Single-constraint experiment changes total continuum absorption in atmospheric profiles. Shown is the change in column-integrated total continuum opacity in the single-constraint experiment ($\tau_{\nu,\mathrm{cont}}$) relative to the baseline experiment ($\tau_{\nu,\mathrm{cont},0}$) for different surface temperatures T_s.

$f_{\mathrm{em,\ foreign}}$ decreases with T_s. Accordingly, a stronger self continuum mostly reduces $\mathcal{L}$ at high T_s, while a stronger foreign continuum mostly reduces $\mathcal{L}$ at low T_s. Hence, $\mathcal{L}$ increases less strongly with T_s when the self continuum is increased but more strongly when the foreign continuum is increased. In other words, the self continuum induces a destabilizing partial feedback while the foreign continuum induces a stabilizing partial feedback. For the same perturbation of ±10% these partial feedbacks in the FIR have roughly the same magnitude at $T_s = 288$ K, while the destabilizing self continuum partial feedback becomes much stronger at higher T_s (Figure 6b).

Furthermore, this framework can also help us understand why the self continuum partial feedback varies among different spectral regions and with T_s. In contrast to the exponential Clausius-Clapeyron relation imposed on water vapor, CO_2 concentration stays constant with T_s in our experiments. Hence, $f_{\mathrm{em,\ self}}$ in the CO_2 band strongly increases with T_s at the cost of CO_2 absorption. Therefore, the destabilizing lapse-rate feedback induced by the self continuum continuously masks more of the stabilizing Planckian response induced by CO_2 at the edges of the 667 cm^{-1} CO_2 band, above $T_s \approx 320$ K this effect even reaches the band center (Figures 4h and 6c).

In the window, $f_{\mathrm{em,self}}$ also increases with T_s along with the self continuum partial feedback. At $T_s \approx 300$ K, however, $f_{\mathrm{em,\ self}} \sim \mathcal{O}(1)$ which means that the self continuum controls most of the emission in the window. Further increasing T_s thus leads to a much weaker increase in $f_{\mathrm{em,self}}$ than below 300 K and thus the self continuum's destabilizing effect weakens (Figure 6d).

Looking at the spectral integral, the effect of variations in the water vapor continuum on λ strongly varies with T_s. At $T_s = 288$ K a 10% stronger self continuum causes λ to become 0.04 W m^{-2} K^{-1} (2%) less negative. This effect continuously increases with T_s and reaches a maximum of around 0.06 W m^{-2} K^{-1} (4%) around 300 K. Varying the foreign continuum by ±10% has a much weaker effect. At T_s below around 295 K the foreign continuum's effect on the surface feedback dominates which causes a destabilizing partial feedback for an increase in foreign continuum absorption, and vice versa. At higher T_s the effect on the atmospheric feedback dominates, which causes a stabilizing partial feedback for an increase in foreign continuum absorption, and vice versa.

4. Effect of Continuum Uncertainty

In the last section we have learned how variations in water vapor self and foreign continuum differently affect both CO_2 forcing $\mathcal{F}$ and longwave feedback λ by varying their magnitude separately. In this section, we build on this understanding and use it to investigate the effect of uncertainty in water vapor continuum absorption.

In order to properly represent this uncertainty, we need to consider that uncertainties in self and foreign continuum are not independent of each other. The foundation for our knowledge of the continuum is formed by field observations and laboratory measurements, both of which rely heavily on measurements of the total continuum. A change in the self continuum is thus usually accompanied by an opposite change in the foreign continuum to restore radiative closure, and thus uncertainties in self and foreign continuum are usually negatively correlated (Delamere et al., 2010; Mlawer et al., 2019, 2023; Mlawer & Turner, 2016; Shine et al., 2016; Turner et al., 2004). To explore the implications of this negative correlation, we consider two different idealized approaches, which are described in more detail in Section 2.5.

4.1. The Single-Constraint Experiment

The purpose of this experiment is to investigate the effect of uncertainty in the surface temperature dependence of the total continuum absorption. We therefore assume that the spectrally resolved total continuum opacity $\tau_{\nu,\ \mathrm{cont}}$ is perfectly constrained at the reference conditions $T_0 = 296$ K, $p_0 = 1013$ hPa, $q_0 = 0.02$ (see Section 2.5.1 for details). Due to the different dependences of self and foreign continuum on T and in particular q, this approach only conserves the total continuum opacity at the given reference conditions. This means that in atmospheres with $q < q_0$, the adjustment of the foreign continuum dominates, increasing the total continuum absorption relative to the baseline simulation. In contrast, in atmospheres with $q > q_0$, the adjustment of the self continuum dominates, decreasing the total continuum absorption (Figure 7).

4.1.1. Effect on CO_2 Forcing

Similar to the separate variations of self and foreign continuum discussed above, the CO_2 forcing $\mathcal{F}$ in the single-constraint experiment mainly changes at the edges of the main CO_2 band (Figure 4m). At surface temperatures $T_s < 310$ K, the stronger foreign continuum dominates which leads to a slightly weaker $\mathcal{F}$; at $T_s > 310$ K the weaker self continuum dominates which leads to a slightly stronger $\mathcal{F}$ (Figure 5d). However, this effect on $\mathcal{F}$ is mostly weaker than ±1%, at $T_s = 288$ K $\mathcal{F}$ is reduced by 0.03 W m^{-2} (0.6%).

4.1.2. Effect on Longwave Feedback

The effect on longwave feedback λ has different signs for different surface temperatures T_s as well (Figures 4n and 5e). At $T_s < 290$ K, the stronger foreign continuum dominates which causes a net destabilizing partial feedback. This mainly occurs because a stronger foreign continuum weakens the surface feedback which more than offsets the strengthening of the surface feedback due to the weaker self continuum (Figures 4g–4k and 4o). However, this changes at $T_s \approx 300$ K, when the effect of the self continuum on the surface feedback becomes dominant (Figures 4o and 5e). At $T_s \approx 315$ K, the surface feedback diminishes, as already described in Section 3.2.

Already at $T_s \approx 290$ K, the stabilizing partial atmospheric feedback becomes stronger than the destabilizing partial surface feedback and thus the net partial feedback becomes stabilizing (Figure 5e). In contrast to the surface feedback, the net effect on the atmospheric feedback is stabilizing throughout the simulated T_s range (Figure 5e). This is because both a weaker self continuum and a stronger foreign continuum cause a stabilizing partial atmospheric feedback (see Section 3.2 and Figures 4h, 4l, and 4p). This effect increases with T_s until around 320 K and stays roughly constant after (Figure 5e).

The strongest effect occurs in the atmospheric window, where the magnitude of λ_{window} is increased by about 0.05 W m^{-2} K^{-1} on average between 290 and 310 K. Because the magnitude of λ_{window} decreases by about 0.05 W m^{-2} K^{-1} per 1 K increase in T_s, the single-constraint experiment lowers the value of T_s at which the atmospheric window closes by about 1 K. Phrased differently, because the opacity τ of continuum absorption continuously increases with T_s (Figure 6 first column), variations in the continuum strength can be thought of as shifting τ in T_s space—and thus also the T_s at which the window closes.

At low T_s the partial feedback is destabilizing (positive) and almost entirely limited to the window. With increasing T_s the partial feedback becomes increasingly stabilizing (negative) throughout the spectrum, also affecting the far-infrared (FIR) water vapor absorption band (Figure 4n). At very high T_s, the partial feedback becomes slightly less stabilizing in the window, while it continues to become more stabilizing in the FIR. This occurs because at those high T_s the continuum controls most of the emission in the window so further increasing T_s has a weaker effect on λ, while this is not the case in the FIR (see Section 3.2 and Figure 6).

Looking at the spectral integral, the effect on λ is modest at $T_s = 288$ K: The destabilizing partial surface feedback and the stabilizing partial atmospheric feedback almost perfectly cancel, leading to a minimally stabilizing effect in λ of only −0.002 W m^{-2} K^{-1} (+0.1%).

In contrast, the single-constraint experiment has a substantial effect at $T_s > 300$ K, where it leads to a stabilizing partial feedback of around −0.07 W m^{-2} K^{-1} (+7%) (dark purple line in Figure 5e). At those T_s the single-constraint experiment has a much stronger effect on λ than a reduction of the self continuum by −10% alone (light blue line in Figure 5e). This can be attributed to the strongly stabilizing effect of increasing the foreign continuum, which is discussed in detail in Section 3.2.

4.1.3. Implications for Climate Sensitivity

The effect on climate sensitivity $\mathcal{S}$ is clearly dominated by the effect on the longwave feedback λ rather than on the CO_2 forcing $\mathcal{F}$ (Figures 5g–5i). At $T_s = 288$ K the effect is modest, with a reduction in $\mathcal{S}$ of only 0.02 K (0.8%). At even lower T_s the slightly destabilizing effect on λ is compensated by its weakening effect on $\mathcal{F}$ which leads to almost no change in $\mathcal{S}$. At higher T_s, however, the single-constraint experiment has a substantial effect: above 300 K the strongly stabilizing effect on λ clearly dominates over the increasing effect on $\mathcal{F}$ which reduces $\mathcal{S}$ by more than 0.2 K (7%).

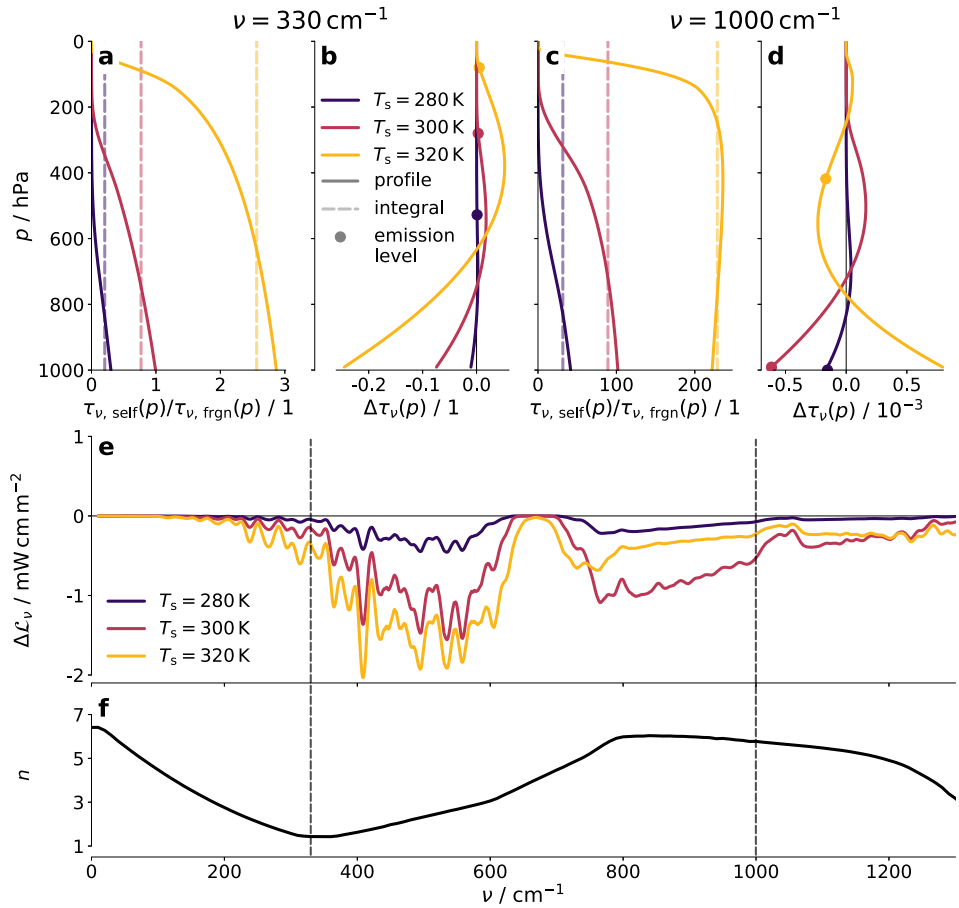

Figure 8. Repartitioning of absorption between self and foreign continuum vertically redistributes atmospheric opacity. Shown are the vertically resolved ratio between opacities of self continuum $\tau_{self}(p)$ and foreign continuum $\tau_{frgn}(p)$ (a, c) and change in total opacity $\Delta\tau(p)$ in the general-constraint experiment with respect to the baseline simulation (b, d) for wavenumbers $\nu = 330$ cm^{-1} (a, b) and $\nu = 1{,}000$ cm^{-1} (c, d), for different surface temperatures T_s. The column-integrated values are shown as light dashed lines and the respective emission levels are shown as solid circles. Also shown are the changes in spectrally resolved outgoing longwave radiation $\Delta\mathcal{L}_\nu$ for the same T_s (e), and the self continuum's temperature dependence exponent n from MT_CKD 4.0 (f).

4.2. The General-Constraint Experiment

The purpose of this experiment is to investigate the effect of uncertainty in the vertical distribution of continuum absorption. We therefore assume that the column-integrated continuum opacity $\tau_{\nu,\text{cont}}$ is perfectly constrained for all of our atmospheric profiles (see Section 2.5.2 for details). However, the redistribution of absorption between self and foreign continuum leads to changes in the vertical profile $\tau_{\nu,\text{cont}}(p)$. This vertical redistribution also occurs in the single-constraint experiment, but the general-constraint experiment allows for an isolation of the effect, without any changes in the column-integrated $\tau_{\nu,\text{cont}}$ with respect to the baseline simulation.

4.2.1. Effect on Outgoing Longwave Radiation

To understand the effect on CO_2 forcing, longwave feedback, and climate sensitivity in the general-constraint experiment, it is helpful to take a step back and first analyze the effect on the outgoing longwave radiation spectrum $\mathcal{L}_\nu$. For almost all T_s, $\mathcal{L}_\nu$ is reduced compared to the baseline simulation, which is caused by changes in the vertical opacity profile $\tau_\nu(p)$. These changes occur because the quadratic dependence of the self continuum on q means that the self continuum is more concentrated in the lower troposphere ("bottom-heavy"), whereas the foreign continuum only depends linearly on q, and thus is somewhat less bottom-heavy. This is demonstrated by the ratio between self and foreign continuum opacity, which generally is highest in the lowest part of the troposphere (Figure 8a). Consequently, by reassigning some of the absorption from the self to the foreign

continuum, opacity is redistributed from the lower to the upper troposphere (Figure 8b), which shifts atmospheric emission toward lower temperatures and thus reduces $\mathcal{L}_\nu$ (Figure 8e).

This reduction of $\mathcal{L}_\nu$ generally increases with T_s because self continuum opacity increases with T_s and thus more opacity is redistributed at higher T_s. However, at $T_s \gg 300$ K, the effect starts to decrease again—first in the window (Figure 8e) but at even higher T_s also in other parts of the spectrum (not shown).

This can be explained by the negative temperature dependence of the self continuum. In the MT_CKD 4.0 model, this is represented as

$$C_{\text{self}}(T) = C_{\text{self}}(296\ \text{K})\left(\frac{296\ \text{K}}{T}\right)^n, \tag{10}$$

where C_{self} is the self continuum absorption cross-section and n is the spectrally varying temperature dependence exponent, which causes the self continuum absorption cross-section to decrease with T (Mlawer et al., 2023, see also Figures 2 and 8f).

Because $\tau_{\text{self}}(T) \propto C_{\text{self}}(T) \cdot q^2(T)$, the ratio $\tau_{\text{self}}/\tau_{\text{foreign}}$ still strongly increases with T_s throughout the troposphere in our experiments. Because of the strongly negative T dependence of C_{self} in the window, the high T in the lower troposphere causes the increase in $\tau_{\text{self}}/\tau_{\text{foreign}}$ with T_s to slow down substantially, while this effect is less pronounced in the cooler upper troposphere. In other words, while $\tau_{\text{self}}/\tau_{\text{foreign}}$ in the window is bottom-heavy at low T_s, it actually peaks at 400 hPa for $T_s = 320$ K (Figure 8c).

Consequently, at sufficiently high T_s, replacing self continuum absorption with foreign continuum absorption becomes less effective in redistributing opacity from the lower to the upper troposphere in the window (Figure 8d). In fact, most of the opacity is distributed from the middle troposphere to the lower troposphere. However, this presumably has no effect on $\mathcal{L}_\nu$ because the emission level in the window is around 400 hPa for $T_s = 320$ K (yellow circle in Figure 8d). Conversely, some opacity is still redistributed from the middle to the upper troposphere. This redistribution reduces $\mathcal{L}_\nu$, but to a lesser extent than at lower T_s (Figure 8e).

4.2.2. Effect on CO_2 Forcing

In the context of CO_2 forcing $\mathcal{F}$, the redistribution of opacity from the lower to the upper troposphere means that this opacity can mask a larger part of the CO_2 absorption spectrum. Analogous to the arguments from Section 3.1 (Jeevanjee, Seeley, et al., 2021), this decreases $\mathcal{F}$ in the general-constraint experiment (Figure 4q). Due to the vertical redistribution of absorption (Section 4.2.1), the effect on $\mathcal{F}$ increases with T_s until around 310 K, and decreases again at higher T_s (Figure 5d). Again, the effect is small in magnitude with around -0.01 W m^{-2} (-0.2%) at 288 K and a maximum effect of -0.025 W m^{-2} (-0.6%) at 310 K.

These results are similar in magintude to the single-constraint experiment, both giving roughly an effect of $\mathcal{O}(1\%)$. However, the two approaches deliver quite different dependences on T_s. While the sign of the effect switches in the single-constraint experiment, it is negative for all T_s in the general-constraint experiment.

4.2.3. Effect on Longwave Feedback

At first glance, the effect on λ_ν in the general-constraint experiment looks somewhat similar to that seen in the single-constraint experiment (Figures 4n and 4r). However, at closer inspection, it becomes clear that those results occur for quite different reasons. In the single-constraint experiment, the positive partial feedback at low T_s was due to the effect on λ_{sfc} (Figure 4o). In the general-constraint experiment, however, the effect on λ_{sfc} is zero by construction (Figure 4s), because λ_{sfc} is only affected by the column-integrated total τ_ν, which is conserved. Rather, the entire effect on λ_ν can be explained by the effect on the atmospheric feedback (Figure 4t).

The reason for this is again the redistribution of absorption from the lower to the upper troposphere, as explained in Section 4.2.1. The consequent reduction in $\mathcal{L}_\nu$ increases with T_s until around 310–320 K, depending on ν, equivalent to a positive partial feedback. At higher T_s, the sign of the partial feedback switches from positive to negative as the $\mathcal{L}_\nu$ reduction starts to decrease with T_s (Figure 5e).

Overall, the effect is in the same order of magnitude as for the single-constraint experiment, both giving effects of $\mathcal{O}(1\%)$ or less at 288 K and up to $\mathcal{O}(5\%)$ above 300 K. However, the two experiments disagree about both the sign of the effect and the exact T_s dependence.

4.2.4. Implications for Climate Sensitivity

The effect on $\mathcal{S}$ is again dominated by the effect on λ, while the effect on $\mathcal{F}$ is much weaker. At 288 K, $\mathcal{S}$ is increased by 0.02 K (1%). The effect on $\mathcal{S}$ reaches a peak of around 0.05 K (2%) at around 300 K. Following the T_s dependence of the effect on λ the sign of the effect on $\mathcal{S}$ switches at around 310 K, reaching a reduction of $\mathcal{S}$ of up to −0.15 K (6%) at 330 K (Figures 5f and 5i).

The two uncertainty experiments disagree on sign and T_s dependence of the effect of continuum uncertainty on $\mathcal{S}$. The difference is most pronounced at around 300 K, where both experiments predict a local maximum of the effect, but of opposite sign. However, they agree that the magnitude of the effect is of $\mathcal{O}(1\%)$ at 288 K and reaches $\mathcal{O}(5\%)$ above 300 K.

5. Discussion

We have developed a careful mechanistic understanding of how uncertainty in the continuum at terrestrial wavenumbers affects CO_2 forcing $\mathcal{F}$, longwave feedback λ, and climate sensitivity $\mathcal{S}$; but how applicable is this to real world uncertainty? In the following, we address the assumptions underlying our idealized representations of atmosphere and spectroscopy and discuss their implications for the generalizability of our results.

5.1. Atmospheric Idealizations

In our representation of the atmosphere, we make two major simplifications, both of which are widely used in idealized single-column studies of Earth's climate (e.g., Jeevanjee, Koll, & Lutsko, 2021; Jeevanjee, Seeley, et al., 2021; Kluft et al., 2021; Koll & Cronin, 2018; Koll et al., 2023; Seeley & Jeevanjee, 2021; Stevens & Kluft, 2023).

First, our single-column approach by design does not account for horizontal variations in temperature and humidity. The main effect of this approach is an underestimation of the effect of continuum uncertainty due to the non-linear dependence of the self continuum on q. To estimate the global mean effect, an average over all T_s weighted by their occurrence on Earth is better suited. The first-order effect of this can be estimated by simply averaging the simulated effects of continuum uncertainty over all T_s that are commonly observed on Earth (270–310 K). This gives an average effect of continuum uncertainty on climate sensitivity of around −0.07 K in the single-constraint experiment and +0.03 K in the general-constraint experiment. Those values are larger than the ±0.02 K found for $T_s = 288$ K, but of similar magnitude, which suggests that this simplification does not qualitatively affect our results. Note that this estimate only captures variations in T_s, but not variations in relative humidity $\mathcal{R}$ at a given T_s which also occur in the real world. To properly account for this, one would need a realistic global climatology of T_s and $\mathcal{R}$, which is beyond the scope of our single-column approach.

Second, we assume a vertically uniform relative humidity profile $\mathcal{R} = 80\%$. This approach overestimates mid-tropospheric $\mathcal{R}$ compared to observational estimates, which generally lie between 40% and 60% (e.g., Sherwood et al., 2010; Wright et al., 2010). However, defining a non-uniform $\mathcal{R}$ profile for a wide range of T_s comes with its own challenges. Defining $\mathcal{R}$ as function of pressure does not capture the vertical expansion of the troposphere as T_s increases, hence it is best practice to define $\mathcal{R}$ as function of temperature instead (Romps, 2014). However, there are many degrees of freedom in choosing a function for $\mathcal{R}$, and the resulting feedback is often sensitive to details in the exact definition of this function (Bourdin et al., 2021). The main effect of assuming a vertically uniform $\mathcal{R}$ profile is an overestimation of the effect of continuum uncertainty due to an overestimation of mid-tropospheric $\mathcal{R}$. To estimate the effect of this assumption, we performed our analysis for an exemplary, and inherently somewhat arbitrary non-uniform $\mathcal{R}$ profile (Figure A1), which is described in more detail in Appendix A. As expected the effect is somewhat reduced in magnitude, but apart from that the results look very similar (Figure A2).

Therefore, rather than trying to capture both horizontal and vertical variations in $\mathcal{R}$ in a realistic way, the goal of this study is to develop a conceptual understanding of how continuum uncertainty propagates to uncertainty in the radiative properties of the Earth. To this end, simplifying assumptions are generally much easier to interpret than

results of more complex experiments, as they help to focus on the essential processes at play. Our conclusions regarding the different mechanisms by which self and foreign continuum affect forcing and feedback at different T_s, as well as the different effects of the two uncertainty experiments, do not seem to be affected by either of these simplifications.

5.2. Spectroscopic Idealizations

Due to the lack of a comprehensive model for continuum uncertainty, we have to rely on idealized representations of this uncertainty. We perform two experiments based on different idealized representations of continuum uncertainty. Both of them are obviously not meant to be perfectly realistic; in fact, they can be considered rather extreme cases that isolate different aspects of continuum uncertainty.

In both approaches, we represent uncertainty by assuming a 10% weaker self continuum compared with MT_CKD 4.0. This is arguably a conservative estimate, particularly in the 1,000 cm^{-1} window, where a number of studies are consistent with a roughly 20% weaker self continuum than in MT_CKD 4.0 (Burch & Alt, 1984; Cormier et al., 2005; Fournier et al., 2024, see also Figure 2). Additional simulations we performed show that the effect of continuum uncertainty is to first order proportional to the assumed magnitude of uncertainty, so the effects of different magnitudes of continuum uncertainty can be estimated from the results presented here. This might also be useful to evaluate how future achievements in reducing continuum uncertainty affect uncertainty in climate sensitivity.

We further assume that continuum uncertainty is spectrally uniform. Given the fact that the continuum in different parts of the spectrum likely originates from different physical processes, this spectral uniformity is unlikely to properly represent actual continuum uncertainty. This caveat thus needs to be considered when interpreting the broadband quantities derived from this assumption.

Similarly, we discard the possibility that the self continuum might be stronger than current estimates because this would violate radiative closure in the windows. Although a stronger self continuum than in MT_CKD 4.0 is unlikely for the arguments outlined above, it cannot be entirely ruled out. However, unless the total continuum absorption in the windows is currently substantially underestimated, this increase in the self continuum would have to be much smaller than 10% in the windows. In that case, the effect on $\mathcal{S}$ would presumably be qualitatively similar to the continuum uncertainty analyzed above, but with opposite sign and substantially reduced magnitude, given that most of the effect of the continuum originates in the window.

Furthermore, we assume that total continuum absorption is perfectly known—under some reference conditions in the single-constraint experiment and even for all atmospheric profiles in the general-constraint experiment. In reality, instrumental errors limit the accuracy of continuum measurements and field studies of the continuum are additionally affected by aerosol effects (e.g., Shine et al., 2016). Both of these effects cause uncertainty in total continuum absorption and thus also in the magnitude of our foreign continuum adjustment. For a weaker adjustment than assumed above, the effect of continuum uncertainty can be estimated qualitatively from Figure 5. The effect would roughly lie in between the case without foreign continuum adjustment (light blue) and either the single-constraint (purple) or general-constraint experiment (orange), respectively. This would imply a weaker effect on $\mathcal{S}$ at high surface temperatures and a still small effect for $T_s = 288$ K. For a stronger adjustment than assumed above, the effect of continuum uncertainty would be even stronger at high surface temperatures.

Moreover, we do not account for uncertainty in the temperature dependence of the self continuum. A recent comparison of different laboratory studies suggests that the negative temperature dependence might be overestimated in MT_CKD 4.0 (Fournier et al., 2024). This can be expected to induce additional uncertainty in $\mathcal{F}$, λ, and $\mathcal{S}$.

For the single-constraint experiment specifically, the choice of the reference values T_0, p_0, and q_0 themselves is to some extent arbitrary. The values we use are chosen to mimic conditions commonly present in both laboratory and field studies of the continuum. Different choices of these reference values, particularly of q_0, have a non-negligible quantitative impact on the effect of continuum uncertainty: For $q_0 = 0.01$, the foreign continuum adjustment is only half as strong compared to $q_0 = 0.02$, which reduces the effect on $\mathcal{S}$ by about one third at high T_s (Figure A2). The biggest effect of q_0 is on the exact T_s at which the effects on $\mathcal{F}$ and λ change sign, while their magnitudes are in many cases quite similar. Regardless of the choice of q_0, the effect of continuum uncertainty on $\mathcal{S}$ is modest for $T_s = 288$ K but substantial at high T_s.

For the general-constraint experiment, the combination of a perfectly constrained total continuum absorption for all T_s and a decrease in the self continuum, which strongly increases with T_s, is a rather extreme case. This is because this combination implies that the foreign continuum increases more strongly with T_s than is supported by our current understanding. This strong increase of the foreign continuum with T_s would either have to come from a stronger-than-linear dependence on q, which contradicts its definition, or from a strongly positive dependence on T, which contradicts the current consensus that the foreign continuum is temperature independent.

Given the limited realism in our representations of continuum uncertainty therefore, the results presented in this study should not be viewed as conclusive quantitative statements on the exact effect of uncertainty in water vapor continuum absorption. However, they give a good picture of the magnitude and temperature dependence of the effect and illuminate the different processes at play.

6. Synthesis

We have developed a conceptual understanding of how uncertainty in water vapor continuum absorption at terrestrial wavenumbers affects CO_2 forcing $\mathcal{F}$, longwave feedback λ, and climate sensitivity $\mathcal{S}$. This understanding is based on simulations that are idealized both in their treatment of the atmosphere and their representation of continuum uncertainty, which allows us to isolate different aspects of the effect of continuum uncertainty and analyze the underlying processes.

Our results highlight in particular the different effects of self and foreign continuum on λ, which arise from their different dependences on water vapor concentration q and temperature T. This has implications for both the dependence of the column-integrated continuum absorption on surface temperature T_s, and the vertical distribution of continuum absorption within the atmospheric column at a given T_s. This demonstrates the importance of a correct partitioning between self and foreign continuum absorption and its relevance for climate studies.

Overall, despite the substantial remaining uncertainty in water vapor continuum absorption at terrestrial wavenumbers, the impact of this uncertainty on $\mathcal{S}$ in our simulations is modest for $T_s = 288$ K. This is the case compared to both the overall uncertainty in $\mathcal{S}$ (Sherwood et al., 2020) and the much smaller uncertainty in the clear-sky longwave $\mathcal{S}$ studied here (Jeevanjee, 2023; Kluft et al., 2019; Manabe & Wetherald, 1967; Stevens & Kluft, 2023). However, continuum uncertainty has a substantial effect on $\mathcal{S}$ at T_s above 300 K. This causes a non-negligible effect in the global mean for present-day climate, but also directly affects the surface temperature dependence of $\mathcal{S}$.

Therefore, a better understanding of the processes that cause the water vapor continuum and better estimates of its magnitude would contribute to further constraining the temperature dependence of $\mathcal{S}$. This temperature dependence is for example, relevant to understand past and possible future climates of Earth, but also those of Venus or Earth-like exoplanets, for example, in the context of the runaway greenhouse effect (e.g., Goldblatt et al., 2013). It could also be useful to interpret estimates of $\mathcal{S}$ based on paleoclimate records from very warm climates such as the Paleocene-Eocene (e.g., Caballero & Huber, 2013). While continuum uncertainty only has a modest impact on $\mathcal{S}$ for $T_s = 288$ K, it does affect estimates of $\mathcal{S}$ in very warm climates. Therefore, continuum uncertainty affects the relationship between $\mathcal{S}$ inferred from those paleoclimate records and $\mathcal{S}$ relevant for contemporary climate change.

For a more quantitative assessment, it would be important to develop a comprehensive model of continuum uncertainty which, to our knowledge, does not currently exist. Such a model would need to not only include the actual uncertainty in self and foreign continuum, but also account for the correlation between the two as a function of temperature and water vapor concentration, covering both terrestrial and solar wavenumbers. Once such a model exists, it will be possible to assess the exact effect of continuum uncertainty under different climate states and the implications for interpreting paleoclimate records. Furthermore, one could then quantify the effect under present-day climate for a realistic global climatology that accounts for horizontal and vertical variations in temperature and humidity, for example, using a general circulation model.

Appendix A: Sensitivity to Idealizations

To investigate the impact of the assumption of a vertically uniform relative humidity profile $\mathcal{R}$, we performed the same analysis as in Section 4.2 for a non-uniform $\mathcal{R}$ profile. We chose a C-shaped $\mathcal{R}$ (Sherwood et al., 2010; Wright et al., 2010), defined as a function of atmospheric temperature T (Romps, 2014). The profile features

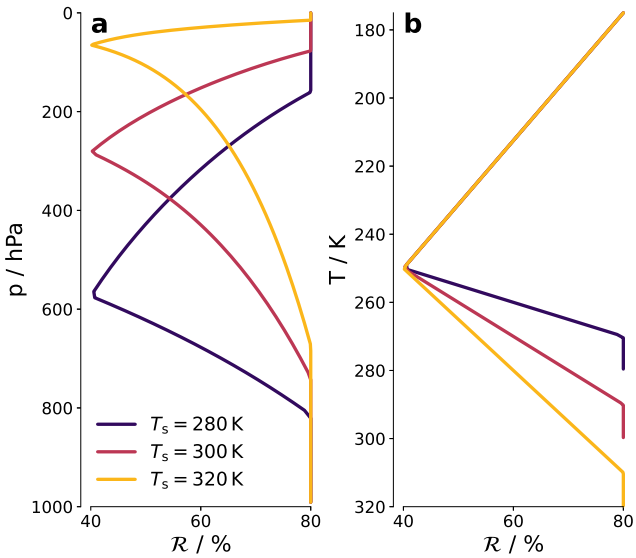

Figure A1. Profiles of relative humidity $\mathcal{R}$ assuming vertically varying $\mathcal{R}$, plotted against pressure p (a) and temperature T (b).

vertically uniform $\mathcal{R} = 80\%$ from the surface to the top of the boundary layer ($T_s - 10$ K). Above the boundary layer, $\mathcal{R}$ first linearly decreases to a minimum of 40% in the mid-troposphere at 250 K, and then linearly increases again to 80% at 175 K. The $\mathcal{R}$ for different T_s are shown as function of p (Figure A1a) and T (Figure A1b).

The effect of this profile on CO_2 forcing $\mathcal{F}$, longwave feedback λ, and climate sensitivity $\mathcal{S}$ is shown in Figure A2. Due to the lower mid-tropospheric $\mathcal{R}$, λ is more negative (Figure A2b), which results in a lower $\mathcal{S}$ (Figure A2c). Regarding the effect of continuum uncertainty, the choice of $\mathcal{R}$ profile mainly affects the single-constraint experiment, where the relative effect on λ and $\mathcal{S}$ are reduced by about a third (Figure A2h,i). For the general-constraint experiment, the effect of continuum uncertainty is only affected for $T_s > 300$ K. Apart from that, the T_s dependence of all quantities is qualitatively very similar to the case of a vertically uniform $\mathcal{R}$ profile.

Finally, the effect of a different choice of $q_0 = 0.01$ for the single-constraint experiment is shown in Figure A2. The effect on λ and $\mathcal{S}$ is increased at $T_s < 295$ K but decreased by up to a third at $T_s > 295$ K compared to the case of $q_0 = 0.02$ (Figures A2h and A2i). Overall, the T_s dependence is again qualitatively similar.

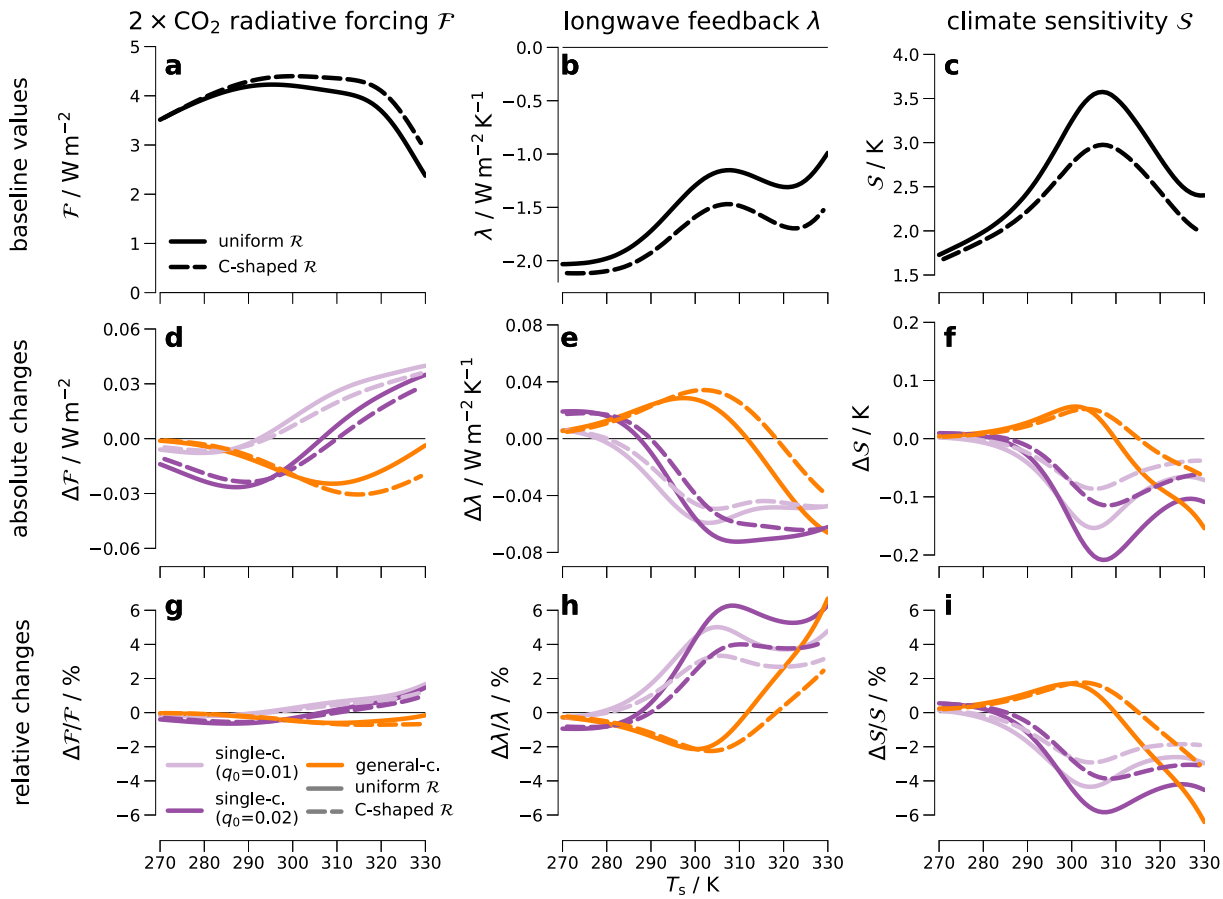

Figure A2. Like Figure 5 but now comparing the single-constraint (purple) and general-constraint (orange) for vertically uniform (solid) and C-shaped (dashed) $\mathcal{R}$ profiles. Additionally, the results of the single-constraint experiment are shown for the choice of $q_0 = 0.01$ (light purple).

Data Availability Statement

Our analysis is based on the konrad model version 1.0.1 (available at https://doi.org/10.5281/zenodo.6046423, Kluft et al., 2022), with some modifications to the model to support the scaling of absorption species (available at https://doi.org/10.5281/zenodo.10961148, Roemer et al., 2024a). For the radiative transfer simulations, we use the ARTS model version 2.6.2 (available at https://doi.org/10.5281/zenodo.10868342, Buehler et al., 2024). The model output produced in this study can be found at https://doi.org/10.5281/zenodo.10963838 (Roemer et al., 2024c), the code needed to run the models and produce the figures of this study can be found at https://doi.org/10.5281/zenodo.10963797 (Roemer et al., 2024b).

Acknowledgments

This work was financially supported by the US National Science Foundation (award AGS-1916908) and by NOAA (award NA20OAR4310375). We acknowledge financial support from the Open Access Publication Fund of Universität Hamburg. This study contributes to the Cluster of Excellence "CLICCS—Climate, Climatic Change, and Society", and to the Center for Earth System Research and Sustainability (CEN) of Universität Hamburg. We want to thank Richard Larsson for developing the ARTS absorption routines, including their representation of the MT_CKD continuum. Our thanks also go to Manfred Brath, Oliver Lemke, and the ARTS radiative transfer community for their help with using ARTS. Finally, we are thankful to the anonymous reviewers and the editor for their constructive comments that helped to improve the manuscript. Open Access funding enabled and organized by Projekt DEAL.

References

Baranov, Y. I., & Lafferty, W. J. (2012). The water vapour self- and water–nitrogen continuum absorption in the 1000 and 2500 cm-1 atmospheric windows. *Philosophical Transactions of the Royal Society A: Mathematical, Physical & Engineering Sciences*, *370*(1968), 2578–2589. https://doi.org/10.1098/rsta.2011.0234

Baranov, Y. I., Lafferty, W. J., Ma, Q., & Tipping, R. H. (2008). Water-vapor continuum absorption in the 800–1250 cm^{-1} spectral region at temperatures from 311 to 363K. *Journal of Quantitative Spectroscopy and Radiative Transfer*, *109*(12), 2291–2302. https://doi.org/10.1016/j.jqsrt.2008.03.004

Bourdin, S., Kluft, L., & Stevens, B. (2021). Dependence of climate sensitivity on the given distribution of relative humidity. *Geophysical Research Letters*, *48*(8), e2021GL092462. https://doi.org/10.1029/2021GL092462

Buehler, S. A., Eriksson, P., Lemke, O., Larsson, R., Pfreundschuh, S., & Brath, M. (2024). ARTS - The atmospheric radiative transfer simulator. *Zenodo*. https://doi.org/10.5281/zenodo.10868342

Buehler, S. A., Mendrok, J., Eriksson, P., Perrin, A., Larsson, R., & Lemke, O. (2018). ARTS, the atmospheric radiative transfer simulator – Version 2.2, the planetary toolbox edition. *Geoscientific Model Development*, *11*(4), 1537–1556. https://doi.org/10.5194/gmd-11-1537-2018

Burch, D. E., & Alt, R. L. (1984). Continuum absorption by H2O in the 700-1200 cm(-1) and 2400-2800 cm(-1) windows. (Technical Report). https://apps.dtic.mil/sti/citations/ADA147391

Caballero, R., & Huber, M. (2013). State-dependent climate sensitivity in past warm climates and its implications for future climate projections. *Proceedings of the National Academy of Sciences*, *110*(35), 14162–14167. https://doi.org/10.1073/pnas.1303365110

Clough, S. A., Kneizys, F. X., & Davies, R. W. (1989). Line shape and the water vapor continuum. *Atmospheric Research*, *23*(3), 229–241. https://doi.org/10.1016/0169-8095(89)90020-3

Cormier, J. G., Hodges, J. T., & Drummond, J. R. (2005). Infrared water vapor continuum absorption at atmospheric temperatures. *The Journal of Chemical Physics*, *122*(11), 114309. https://doi.org/10.1063/1.1862623

Dacie, S., Kluft, L., Schmidt, H., Stevens, B., Buehler, S. A., Nowack, P. J., et al. (2019). A 1D RCE study of factors affecting the tropical tropopause layer and surface climate. *Journal of Climate*, *32*(20), 6769–6782. https://doi.org/10.1175/JCLI-D-18-0778.1

Delamere, J. S., Clough, S. A., Payne, V. H., Mlawer, E. J., Turner, D. D., & Gamache, R. R. (2010). A far-infrared radiative closure study in the Arctic: Application to water vapor. *Journal of Geophysical Research*, *115*(D17). https://doi.org/10.1029/2009JD012968

Eng, R. S., & Mantz, A. W. (1980). Tunable diode laser measurements of water vapor continuum and water vapor absorption line shape in the 10 μm atmospheric transmission window region. In *Atmospheric water vapor* (pp. 101–111). Elsevier.

Eriksson, P., Buehler, S. A., Davis, C. P., Emde, C., & Lemke, O. (2011). ARTS, the atmospheric radiative transfer simulator, version 2. *Journal of Quantitative Spectroscopy and Radiative Transfer*, *112*(10), 1551–1558. https://doi.org/10.1016/j.jqsrt.2011.03.001

Feng, J., Paynter, D., & Menzel, R. (2023). How a stable greenhouse effect on Earth is maintained under global warming. *Journal of Geophysical Research: Atmospheres*, *128*(9), e2022JD038124. https://doi.org/10.1029/2022JD038124

Foote, E. (1856). ART. XXXI.–Circumstances affecting the heat of the Sun's Rays: (Read before the American association, August 23d, 1856.). *American Journal of Science and Arts*, *22*(66), 382. Retrieved from https://www.proquest.com/docview/89589867/abstract/741F2910EDED4903PQ/1

Fournier, Q., Kassi, S., Mondelain, D., Fleurbaey, H., Georges, R., & Campargue, A. (2024). The water vapor self-continuum absorption at 8.45 µm by optical feedback cavity ring down spectroscopy. *Journal of Quantitative Spectroscopy and Radiative Transfer*, *315*, 108875. https://doi.org/10.1016/j.jqsrt.2023.108875

Goldblatt, C., Robinson, T. D., Zahnle, K. J., & Crisp, D. (2013). Low simulated radiation limit for runaway greenhouse climates. *Nature Geoscience*, *6*(8), 661–667. https://doi.org/10.1038/ngeo1892

Gordon, I. E., Rothman, L. S., Hargreaves, R. J., Hashemi, R., Karlovets, E. V., Skinner, F. M., et al. (2022). The HITRAN2020 molecular spectroscopic database. *Journal of Quantitative Spectroscopy and Radiative Transfer*, *277*, 107949. https://doi.org/10.1016/j.jqsrt.2021.107949

Hinderling, J., Sigrist, M. W., & Kneubühl, F. K. (1987). Laser-photoacoustic spectroscopy of water-vapor continuum and line absorption in the 8 to 14 μm atmospheric window. *Infrared Physics*, *27*(2), 63–120. https://doi.org/10.1016/0020-0891(87)90013-3

Ingram, W. (2010). A very simple model for the water vapour feedback on climate change. *Quarterly Journal of the Royal Meteorological Society*, *136*(646), 30–40. https://doi.org/10.1002/qj.546

Jeevanjee, N. (2023). Climate sensitivity from radiative-convective equilibrium: A chalkboard approach. *American Journal of Physics*, *91*(9), 731–745. https://doi.org/10.1119/5.0135727

Jeevanjee, N., Koll, D. D. B., & Lutsko, N. (2021). "Simpson's Law" and the spectral cancellation of climate feedbacks. *Geophysical Research Letters*, *48*(14), e2021GL093699. https://doi.org/10.1029/2021GL093699

Jeevanjee, N., Seeley, J. T., Paynter, D., & Fueglistaler, S. (2021). An analytical model for spatially varying clear-sky CO_2 forcing. *Journal of Climate*, *34*(23), 9463–9480. https://doi.org/10.1175/JCLI-D-19-0756.1

Kiehl, J. T., & Ramanathan, V. (1982). Radiative heating due to increased CO_2: The role of H_2O continuum absorption in the 12–18 μm region. *Journal of the Atmospheric Sciences*, *39*(12), 2923–2926. https://doi.org/10.1175/1520-0469(1982)039⟨2923:RHDTIC⟩2.0.CO;2

Kluft, L., Dacie, S., & Bourdin, S. (2022). atmtools/konrad: Fix ARTS and cloud interfaces. *Zenodo*. https://doi.org/10.5281/zenodo.6046423

Kluft, L., Dacie, S., Brath, M., Buehler, S. A., & Stevens, B. (2021). Temperature-dependence of the clear-sky feedback in radiative-convective equilibrium. *Geophysical Research Letters*, *48*(22), e2021GL094649. https://doi.org/10.1029/2021GL094649

Kluft, L., Dacie, S., Buehler, S. A., Schmidt, H., & Stevens, B. (2019). Re-examining the first climate models: Climate sensitivity of a modern radiative–convective equilibrium model. *Journal of Climate*, *32*(23), 8111–8125. https://doi.org/10.1175/JCLI-D-18-0774.1

Koll, D. D. B., & Cronin, T. W. (2018). Earth's outgoing longwave radiation linear due to H_2O greenhouse effect. *Proceedings of the National Academy of Sciences*, *115*(41), 10293–10298. https://doi.org/10.1073/pnas.1809868115

Koll, D. D. B., Jeevanjee, N., & Lutsko, N. J. (2023). An analytic model for the clear-sky longwave feedback. *Journal of the Atmospheric Sciences*, *1*(aop), 1923–1951. https://doi.org/10.1175/JAS-D-22-0178.1

Liuzzi, G., Masiello, G., Serio, C., Palchetti, L., & Bianchini, G. (2014). Validation of H_2O continuum absorption models in the wave number range 180–600 cm^{-1} with atmospheric emitted spectral radiance measured at the Antarctica Dome-C site. *Optics Express*, *22*(14), 16784–16801. https://doi.org/10.1364/OE.22.016784

Loper, G. L., O'Neill, M. A., & Gelbwachs, J. A. (1983). Water-vapor continuum CO_2 laser absorption spectra between 27°C and −10°C. *Applied Optics*, *22*(23), 3701–3710. https://doi.org/10.1364/AO.22.003701

Ma, Q., & Tipping, R. H. (1991). A far wing line shape theory and its application to the water continuum absorption in the infrared region. I. *The Journal of Chemical Physics*, *95*(9), 6290–6301. https://doi.org/10.1063/1.461549

Manabe, S., & Wetherald, R. T. (1967). Thermal equilibrium of the atmosphere with a given distribution of relative humidity. *Journal of the Atmospheric Sciences*, *24*(3), 241–259. https://doi.org/10.1175/1520-0469(1967)024⟨0241:TEOTAW⟩2.0.CO;2

Meraner, K., Mauritsen, T., & Voigt, A. (2013). Robust increase in equilibrium climate sensitivity under global warming. *Geophysical Research Letters*, *40*(22), 5944–5948. https://doi.org/10.1002/2013GL058118

Mlawer, E. J., Cady-Pereira, K. E., Mascio, J., & Gordon, I. E. (2023). The inclusion of the MT_ckd water vapor continuum model in the HITRAN molecular spectroscopic database. *Journal of Quantitative Spectroscopy and Radiative Transfer*, *306*, 108645. https://doi.org/10.1016/j.jqsrt.2023.108645

Mlawer, E. J., & Turner, D. D. (2016). Spectral radiation measurements and analysis in the ARM program. *Meteorological Monographs*, *57*(1), 14.1–14.17. https://doi.org/10.1175/AMSMONOGRAPHS-D-15-0027.1

Mlawer, E. J., Turner, D. D., Paine, S. N., Palchetti, L., Bianchini, G., Payne, V. H., et al. (2019). Analysis of water vapor absorption in the far-infrared and submillimeter regions using surface radiometric measurements from extremely dry locations. *Journal of Geophysical Research: Atmospheres*, *124*(14), 8134–8160. https://doi.org/10.1029/2018JD029508

Mukhopadhyay, A., Cole, W. T. S., & Saykally, R. J. (2015). The water dimer I: Experimental characterization. *Chemical Physics Letters*, *633*, 13–26. https://doi.org/10.1016/j.cplett.2015.04.016

Newman, S. M., Green, P. D., Ptashnik, I. V., Gardiner, T. D., Coleman, M. D., McPheat, R. A., & Smith, K. M. (2012). Airborne and satellite remote sensing of the mid-infrared water vapour continuum. *Philosophical Transactions of the Royal Society A: Mathematical, Physical & Engineering Sciences*, *370*(1968), 2611–2636. https://doi.org/10.1098/rsta.2011.0223

Nordstrom, R. J., Thomas, M. E., Peterson, J. C., Damon, E. K., & Long, R. K. (1978). Effects of oxygen addition on pressure-broadened water-vapor absorption in the 10-microm region. *Applied Optics*, *17*(17), 2724–2729. https://doi.org/10.1364/AO.17.002724

Odintsova, T. A., Koroleva, A. O., Simonova, A. A., Campargue, A., & Tretyakov, M. Y. (2022). The atmospheric continuum in the "terahertz gap" region (15–700 cm^{-1}): Review of experiments at SOLEIL synchrotron and modeling. *Journal of Molecular Spectroscopy*, *386*, 111603. https://doi.org/10.1016/j.jms.2022.111603

Paynter, D. J., Ptashnik, I. V., Shine, K. P., Smith, K. M., McPheat, R., & Williams, R. G. (2009). Laboratory measurements of the water vapor continuum in the 1200–8000 cm^{-1} region between 293 K and 351 K. *Journal of Geophysical Research*, *114*(D21). https://doi.org/10.1029/2008JD011355

Paynter, D. J., & Ramaswamy, V. (2011). An assessment of recent water vapor continuum measurements upon longwave and shortwave radiative transfer. *Journal of Geophysical Research*, *116*(D20), D20302. https://doi.org/10.1029/2010JD015505

Paynter, D. J., & Ramaswamy, V. (2012). Variations in water vapor continuum radiative transfer with atmospheric conditions: Water vapor continuum energy budget. *Journal of Geophysical Research*, *117*(D16). https://doi.org/10.1029/2012JD017504

Peterson, J. C., Thomas, M. E., Nordstrom, R. J., Damon, E. K., & Long, R. K. (1979). Water vapor-nitrogen absorption at CO(2) laser frequencies. *Applied Optics*, *18*(6), 834–841. https://doi.org/10.1364/AO.18.000834

Pierrehumbert, R. T. (2010). *Principles of planetary climate*. Cambridge University Press. (Google-Books-ID: bO_U8f5pVR8C).

Ptashnik, I., Shine, K., & Vigasin, A. (2011). Water vapour self-continuum and water dimers: 1. Analysis of recent work. *Journal of Quantitative Spectroscopy and Radiative Transfer*, *112*(8), 1286–1303. https://doi.org/10.1016/j.jqsrt.2011.01.012

Roemer, F. E., Buehler, S. A., Kluft, L., & Pincus, R. (2024a). Git Patches to modify Konrad to support scaling of absorption species in line-by-line calculations (Version 3) [Software]. *Zenodo*. https://doi.org/10.5281/zenodo.10961148

Roemer, F. E., Buehler, S. A., Kluft, L., & Pincus, R. (2024b). Supplementary data for "effect of uncertainty in water vapor continuum absorption on CO_2 forcing, longwave feedback, and climate sensitivity" (version 3) [Dataset]. *Zenodo*. https://doi.org/10.5281/zenodo.10963797

Roemer, F. E., Buehler, S. A., Kluft, L., & Pincus, R. (2024c). Supplementary code for "effect of uncertainty in water vapor continuum absorption on CO_2 forcing, longwave feedback, and climate sensitivity" (version 3) [Software]. *Zenodo*. https://doi.org/10.5281/zenodo.10963838

Romps, D. M. (2014). An analytical model for tropical relative humidity. *Journal of Climate*, *27*(19), 7432–7449. https://doi.org/10.1175/JCLI-D-14-00255.1

Romps, D. M. (2020). Climate sensitivity and the direct effect of carbon dioxide in a limited-area cloud-resolving model. *Journal of Climate*, *33*(9), 3413–3429. https://doi.org/10.1175/JCLI-D-19-0682.1

Seeley, J. T., & Jeevanjee, N. (2021). H2O windows and CO_2 radiator fins: A clear-sky explanation for the peak in equilibrium climate sensitivity. *Geophysical Research Letters*, *48*(4), e2020GL089609. https://doi.org/10.1029/2020GL089609

Serio, C., Masiello, G., Esposito, F., Girolamo, P. D., Iorio, T. D., Palchetti, L., et al. (2008). Retrieval of foreign-broadened water vapor continuum coefficients from emitted spectral radiance in the H_2O rotational band from 240 to 590 cm^{-1}. *Optics Express*, *16*(20), 15816–15833. https://doi.org/10.1364/OE.16.015816

Sherwood, S. C., Ingram, W., Tsushima, Y., Satoh, M., Roberts, M., Vidale, P. L., & O'Gorman, P. A. (2010). Relative humidity changes in a warmer climate. *Journal of Geophysical Research*, *115*(D9). https://doi.org/10.1029/2009JD012585

Sherwood, S. C., Webb, M. J., Annan, J. D., Armour, K. C., Forster, P. M., Hargreaves, J. C., et al. (2020). An assessment of Earth's climate sensitivity using multiple lines of evidence. *Reviews of Geophysics*, *58*(4), e2019RG000678. https://doi.org/10.1029/2019RG000678

Shine, K. P., Campargue, A., Mondelain, D., McPheat, R. A., Ptashnik, I. V., & Weidmann, D. (2016). The water vapour continuum in near-infrared windows – Current understanding and prospects for its inclusion in spectroscopic databases. *Journal of Molecular Spectroscopy*, *327*, 193–208. https://doi.org/10.1016/j.jms.2016.04.011

Shine, K. P., Ptashnik, I. V., & Rädel, G. (2012). The water vapour continuum: Brief history and recent developments. *Surveys in Geophysics*, *33*(3), 535–555. https://doi.org/10.1007/s10712-011-9170-y

Simpson, G. (1928a). Further studies in terrestrial radiation. *Quarterly Journal of the Royal Meteorological Society*, *3*(8), 1–26. https://doi.org/10.1175/1520-0493(1928)56<322:fsitr>2.0.co;2

Simpson, G. (1928b). Some studies in terrestrial radiation. *Quarterly Journal of the Royal Meteorological Society*, *2*, 69–95.

Stevens, B., & Kluft, L. (2023). *A colorful look at climate sensitivity* (pp. 1–24). EGUsphere. https://doi.org/10.5194/egusphere-2022-1460

Taylor, J. P., Newman, S. M., Hewison, T. J., & McGrath, A. (2003). Water vapour line and continuum absorption in the thermal infrared—Reconciling models and observations. *Quarterly Journal of the Royal Meteorological Society*, *129*(594), 2949–2969. https://doi.org/10.1256/qj.03.08

Tipping, R. H., & Ma, Q. (1995). Theory of the water vapor continuum and validations. *Atmospheric Research*, *36*(1), 69–94. https://doi.org/10.1016/0169-8095(94)00028-C

Turner, D. D., Tobin, D. C., Clough, S. A., Brown, P. D., Ellingson, R. G., Mlawer, E. J., et al. (2004). The QME AERI LBLRTM: A closure experiment for downwelling high spectral resolution infrared radiance. *Journal of the Atmospheric Sciences*, *61*(22), 2657–2675. https://doi.org/10.1175/JAS3300.1

Tyndall, J. (1861a). XXIII. On the absorption and radiation of heat by gases and vapours, and on the physical connexion of radiation, absorption, and conduction.—The Bakerian lecture. *The London, Edinburgh and Dublin Philosophical Magazine and Journal of Science*, *22*(146), 169–194. https://doi.org/10.1080/14786446108643138

Tyndall, J. (1861b). XXXVI. On the absorption and radiation of heat by gases and vapours, and on the physical connexion of radiation, absorption, and conduction.—The Bakerian lecture. *The London, Edinburgh and Dublin Philosophical Magazine and Journal of Science*, *22*(147), 273–285. https://doi.org/10.1080/14786446108643154

Vigasin, A. A. (2000). Water vapor continuous absorption in various mixtures: Possible role of weakly bound complexes. *Journal of Quantitative Spectroscopy and Radiative Transfer*, *64*(1), 25–40. https://doi.org/10.1016/S0022-4073(98)00142-3

Wing, A. A., Reed, K. A., Satoh, M., Stevens, B., Bony, S., & Ohno, T. (2018). Radiative–convective equilibrium model intercomparison project. *Geoscientific Model Development*, *11*(2), 793–813. https://doi.org/10.5194/gmd-11-793-2018

Wright, J. S., Sobel, A., & Galewsky, J. (2010). Diagnosis of zonal mean relative humidity changes in a warmer climate. *Journal of Climate*, *23*(17), 4556–4569. https://doi.org/10.1175/2010JCLI3488.1